Journal of
Medicinal Chemistry

Article

Start selective and rigidify: The discovery path towards a next generation of EGFR tyrosine kinase inhibitors.

Harald Engelhardt, Dietrich Böse, Mark Petronczki, Dirk Scharn, Gerd Bader, Anke Baum, Andreas Bergner, Eugene Chong, Sandra Döbel, Georg Egger, Christian Engelhardt, Peter Ettmayer, Julian E. Fuchs, Thomas Gerstberger, Nina C. Gonnella, Andreas Grimm, Elisabeth Grondal, Nizar Haddad, Barbara Hopfgartner, Roland Kousek, Mariusz Krawiec, Monika Kriz, Lyne Lamarre, Joyce Leung, Moriz Mayer, Nitinchandra D Patel, Biljana Peric Simov, Jonathan T. Reeves, Renate Schnitzer, Andreas Schrenk, Bernadette Sharps, Flavio Solca, Heinz Stadtmüller, Zhulin Tan, Tobias Wunberg, Andreas Zöphel, and Darryl B. McConnell

J. Med. Chem., **Just Accepted Manuscript** • DOI: 10.1021/acs.jmedchem.9b01169 • Publication Date (Web): 05 Nov 2019

Just Accepted

is published by the American Chemical Society. 1155 Sixteenth Street N.W., Washington, DC 20036

	Signaling Lamarre, Lyne; Boehringer Ingelheim RCV GmbH & Co KG, Cancer Cell Signaling Leung, Joyce; Boehringer Ingelheim Pharmaceuticals Inc, Chemical Development Mayer, Moriz; Boehringer Ingelheim RCV GmbH und Co KG, Medicinal Chemistry Patel, Nitinchandra; Boehringer Ingelheim Pharmaceuticals Inc, Chemical Development Peric Simov, Biljana; Boehringer Ingelheim RCV GmbH & Co KG, Medicinal Chemistry Reeves, Jonathan; Boehringer Ingelheim, Chemical Development Schnitzer, Renate; Boehringer Ingelheim RCV GmbH & Co KG, Cancer Cell Signaling Schrenk, Andreas; Boehringer Ingelheim RCV GmbH & Co KG, Cancer Cell Signaling Sharps, Bernadette; Boehringer Ingelheim RCV GmbH & Co KG, Cancer Cell Signaling Solca, Flavio; Boehringer Ingelheim RCV GmbH & Co KG, Cancer Pharmacology & Translational Research Stadtmüller, Heinz; Boehringer Ingelheim RCV GmbH & Co KG, Medicinal Chemistry Tan, Zhulin; Boehringer Ingelheim, Chemical Development Wunberg, Tobias; Boehringer Ingelheim RCV GmbH & Co KG, Medicinal Chemistry Zöphel, Andreas; Boehringer Ingelheim RCV GmbH & Co KG, Medicinal Chemistry McConnell, Darryl; Boehringer Ingelheim RCV GmbH & Co KG, Medicinal Chemistry

Start selective and rigidify: The discovery path towards a next generation of EGFR tyrosine kinase inhibitors.

Harald Engelhardt[1]‡, Dietrich Böse[1]†‡, Mark Petronczki[1], Dirk Scharn[1], Gerd Bader[1], Anke Baum[1], Andreas Bergner[1], Eugene Chong[2], Sandra Döbel[1], Georg Egger[1], Christian Engelhardt[1], Peter Ettmayer[1], Julian E. Fuchs[1], Thomas Gerstberger[1], Nina Gonnella[2], Andreas Grimm[1], Elisabeth Grondal[1], Nizar Haddad[2], Barbara Hopfgartner[1], Roland Kousek[1], Mariusz Krawiec[2], Monika Kriz[1], Lyne Lamarre[1], Joyce Leung[2],Moriz Mayer[1], Nitinchandra D. Patel[2], Biljana Peric Simov[1], Jonathan T. Reeves[2], Renate Schnitzer[1], Andreas Schrenk[1], Bernadette Sharps[1], Flavio Solca[1], Heinz Stadtmüller[1], Zhulin Tan[2], Tobias Wunberg[1], Andreas Zoephel[1], Darryl B. McConnell[1]*

[1]Boehringer Ingelheim RCV GmbH & Co KG, Dr-Boehringer-Gasse 5-11, 1120 Vienna, Austria

[2]Boehringer Ingelheim Pharmaceuticals, Inc., 900 Ridgebury Road, Ridgefield,

Connecticut 06877, United States

ABSTRACT

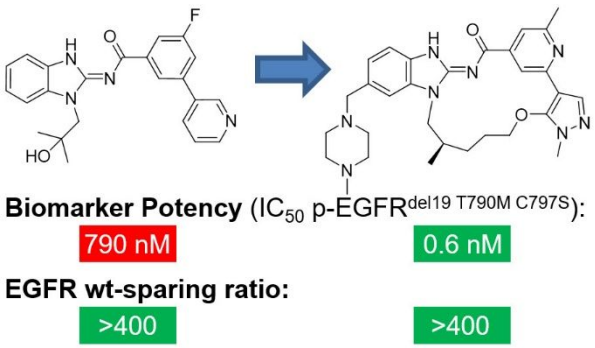

The epidermal growth factor receptor (EGFR), when carrying an activating mutation like del19 or L858R, acts as an oncogenic driver in a subset of lung tumors. While tumor responses to tyrosine kinase inhibitors (TKIs) are accompanied by marked tumor shrinkage, the response is usually not durable. Most patients relapse within two years of therapy often due to acquisition of an additional mutation in EGFR kinase domain that confers resistance to TKIs. Crucially, oncogenic EGFR harboring both resistance mutations, T790M and C797S, can no longer be inhibited by currently approved EGFR TKIs. Here, we describe the discovery of **BI-4020,** which is a non-covalent, wild-type EGFR sparing, macrocyclic TKI. **BI-4020** potently inhibits the above described EGFR variants and induces tumor regressions in a cross-resistant EGFR$^{del19\ T790M\ C797S}$ xenograft model. Key was the identification of a highly selective but moderately potent

benzimidazole followed by complete rigidification of the molecule through macrocyclization.

INTRODUCTION

Kinases are one of the most successfully pursued drug target families with more than 50 kinase inhibitors approved by the FDA to date.[1] Despite this success, discovering kinase inhibitors with a sufficiently high degree of kinome selectivity and hence tolerability remains a significant challenge to medicinal chemists.[2, 3] This challenge is exacerbated in oncology by the emergence of drug resistance which requires next generation inhibitors that are able to inhibit both primary and resistant oncogenic clones while maintaining kinome selectivity.[4-7] New approaches for the discovery of highly selective kinase inhibitors have emerged such as the screening of libraries of kinase inhibitors with intrinsic selectivity profiles[8, 9] and macrocyclization of kinase inhibitors.[10, 11]

The epidermal growth factor receptor (EGFR) is a receptor tyrosine kinase that transduces mitogenic signals. Mutations in the EGFR gene are found in approximately 12 % to 47 % of non-small cell lung cancer (NSCLC) tumors with adenocarcinoma histology.[12] The two most frequent EGFR alterations found in NSCLC tumors are short in-frame deletions in exon 19 (del19) of the EGFR gene and L858R, a single missense

mutation in exon 21.[13] These two mutations cause ligand-independent EGFR activation and are collectively referred to as $EGFR^{M+}$. Del19 and L858R mutations in EGFR sensitize NSCLC tumors to the treatment with EGFR tyrosine kinase inhibitors (TKIs). Clinical experience shows that the objective response rate in lung cancer patients carrying tumors with $EGFR^{M+}$ is approximately 60-85 % in 1st line with the 1st, 2nd and 3rd generation EGFR TKIs erlotinib, gefitinib, afatinib and osimertinib (structures see **Figure 1**).[14-17] These responses demonstrate that $EGFR^{M+}$ NSCLC cells and tumors depend on oncogenic EGFR activity for survival and proliferation, establishing del19 or L858R mutated EGFR variants as a validated drug targets and predictive biomarkers for the treatment of NSCLC.

While tumor responses are accompanied by marked tumor shrinkage in patients, the response is usually not durable, and most patients relapse within 9.2 to 14.7 months of treatment with 1st and 2nd generation EGFR TKIs.[14-18] The most prominent molecular resistance mechanism associated with disease progression in 50% to 70% of patients treated with 1st and 2nd generation EGFR inhibitors is the acquisition of a secondary

mutation in EGFR, namely the gatekeeper mutation T790M.[19, 20] This mutation attenuates the inhibitory activity of 1st and 2nd generation TKIs in cellular assays. EGFR wild-type sparing covalent 3rd generation EGFR TKIs, such as osimertinib, have been developed that effectively inhibit the primary EGFR mutations del19 and L858R independent of the presence or absence of the secondary T790M resistance mutation.[21, 22]

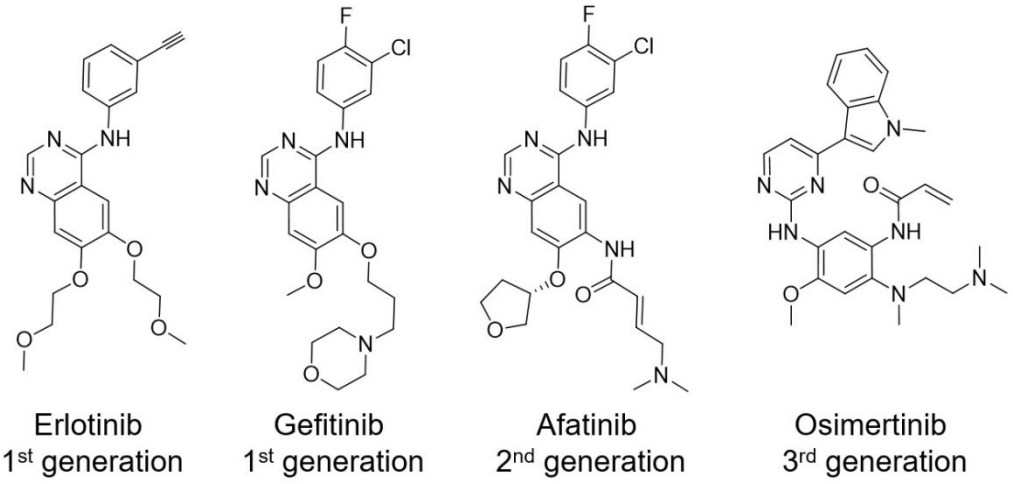

Figure 1. Overview of selected approved 1st, 2nd and 3rd generation EGFR TKIs.

While osimertinib in 2nd line treatment of EGFR M^+ T790M-positive NSCLC patients demonstrates clear clinical efficacy[23, 24] disease progression occurs after an average duration of 10 months.[24] Recent data suggest that 20-40% of 2nd line patients relapsing

on osimertinib TKI[25-29] acquire a tertiary EGFR mutation at the cysteine residue (C797S) required for covalent inhibitor binding.[21, 22] Crucially, the EGFR del19/L858R T790M C797S cis mutant kinase variant that emerges in 2nd line patients progressing on osimertinib[25-29] can no longer be inhibited by any of the approved 1st, 2nd or 3rd generation EGFR TKIs.[27] While the EGFR resistance mutation spectrum after 1st line osimertinib treatment has not been extensively studied, first available data also suggest the emergence of the C797S mutation.[30] Hence, the next generation of EGFR TKIs should be (a) highly active against most common EGFR activation mutation del19, (b) not be susceptible to the most common resistance mutations T790M and/or C797S, (c) have low inhibition of $EGFR^{wt}$ to avoid on-target toxicities such as rash and diarrhea and (d) be highly selective across the human kinome.

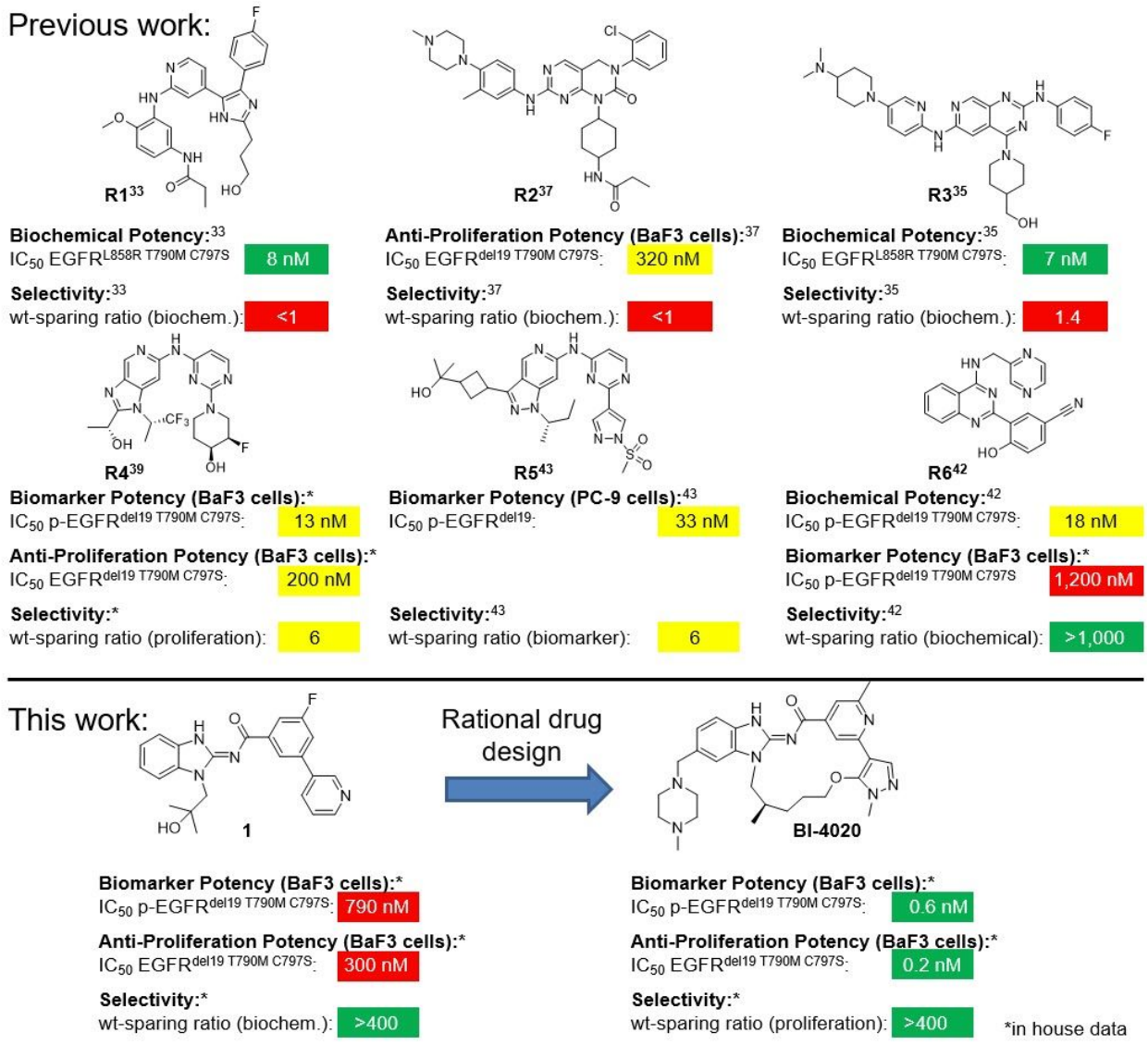

Figure 2. Overview of selected published EGFR inhibitors with inhibition data (**R1 = 31b**[33]; **R2 = JND3229**[37]; **R3 = B30**[35]; **R4 = 42**[39]; **R5 = 21**[43] and **R6 = 19**[42]). Compound **1** serves as starting point for this work and **BI-4020** demonstrates the superiority of the compounds reported by this work compared to state of the art.

Recently, a number of potent EGFR inhibitors able to overcome EGFR T790M and C797S resistance mutations were reported[31-44] but these compounds are equipotent or

more active on $EGFR^{wt}$ (see **R1-3** in **Figure 2**).[31-38] Conversely, some cases of good selectivity for mutated versus wild-type EGFR have been reported but with low overall in vitro potency (see **R4** and **R6** in **Figure 2)**.[40-42] The non-covalent inhibitor **R5**[43] has demonstrated acceptable p-EGFR biomarker modulation *in-vivo* in a NCI-H1975 xenograft model ($EGFR^{L858R\ T790M}$) after high oral dose administration, but the compound displays an insufficient EGFR wt-sparing ratio. Allosteric EGFR inhibitors which overcome T790M and C797S resistance and display EGFR wt-sparing behavior have been reported,[45-49] but these compounds are only active on the L858R mutant but not on the most prevalent del19 mutant.

In this paper, we describe the discovery of **BI-4020**, the first compound to exhibit a next generation EGFR TKI profile, wt-sparing, capable of inhibiting complex EGFR mutations containing T790M and/or C797S modifications, including a triple cis mutation in the $EGFR^{del19}$ background. Key to the discovery was the identification of a highly selective but moderately potent benzimidazole by screening our corporate selective kinase inhibitor library followed by complete rigidification of the molecule through macrocyclization. **BI-**

4020 is a non-covalent, macrocyclic TKI which inhibits not only the triple mutant $EGFR^{del19\ T790M\ C797S}$ variant but also the double mutant $EGFR^{del19\ T790M}$ and primary mutant $EGFR^{del19}$ whilst sparing activity against $EGFR^{wt}$ (see **Figure 2** and **Table 4**). **BI-4020** shows high potency on EGFR mutant cells, high kinome selectivity and good DMPK properties which led to tumor regressions in the human PC-9 ($EGFR^{del19\ T790M\ C797S}$) triple mutant NSCLC xenograft model in mice.

RESULTS AND DISCUSSION

Selectivity 1st: Screening for a highly selective rather than a highly active starting point.

At the outset of the project we decided to start a screening campaign to find chemical starting points which provided selectivity for the mutated EGFR proteins over $EGFR^{wt}$ protein rather than a high activity. We hypothesized that it would be easier to improve upon the activity of an $EGFR^{wt}$ selective molecule than it would be to rationally design in $EGFR^{wt}$ selectivity of a potent but unselective inhibitor. A structure-based design approach to generate selectivity for the EGFR primary activation mutation L858R and del19 over $EGFR^{wt}$ was further ruled out as no structural differences between the binding pockets from the publicly available x-ray structures of the $EGFR^{L858R}$ and $EGFR^{wt}$ proteins were observable.

Instead, we resolved to design a focused in-house library based on Boehringer Ingelheim kinase selectivity panel data obtained with previous research compounds from various projects. Focusing on selective kinase inhibitors where more than 10 mg solid was in stock and that fulfilled minimal drug like properties (heavy atoms ≤ 34 or soluble

at pH 6.8), we compiled a list of 1,826 kinase inhibitors from 40 past kinase and 47 non-kinase projects. A compound, which qualifies as a selective kinase inhibitor needs to be tested against at least 30 kinases and should be active in at least 2 assays (single concentration measurement using a biochemical kinase assay; compound need to display a value a value blow 50% of control) but should not hit more than 10% of all tested kinases. Interestingly, this Selective Kinase Inhibitor (SKIny) Screening Library covered 269 kinases.

Despite the fact that we were most interested in the more frequent appearing $EGFR^{del19\ T790M\ C797S}$ mutation, the triple mutant $EGFR^{L858R\ T790M\ C979S}$ protein was used for the biochemical screening assay, because we were not able to obtain sufficient high quality amounts of the $EGFR^{del19\ T790M\ C797S}$ protein. In parallel to an activity screening, we conducted a selectivity screening using the $EGFR^{wt}$ protein in order to directly assess the WT-sparing effect of the hits found in the screen. The aminobenzimidazole **1** was identified as a promising hit from the screen as it showed reasonable affinity to mutated EGFR (IC_{50} $EGFR^{L858R\ T790M\ C797S}$ = 2,100 nM); IC_{50} $EGFR^{del19\ T790M\ C797S}$ = 250 nM) and had no measurable affinity to $EGFR^{wt}$ (see **Table 1**). In order to assess the overall kinase

selectivity of **1** we performed a kinase selectivity assay[50] with 238 kinases and found that only 5% of the screened kinases were inhibited above 70%. In order to determine the overall kinase selectivity for further compounds more quickly, we have defined a diverse set of 30 kinases representing the kinome. For key compounds **1**, **3** and **BI-4020** we have confirmed the results of the small panel with a larger set of kinases (see **Table 1** and **2**). Gratifyingly, we were also already able to measure biomarker modulation in an $EGFR^{del19\ T790M\ C797S}$ dependent BaF3 cell line with an IC_{50} = 790 nM.

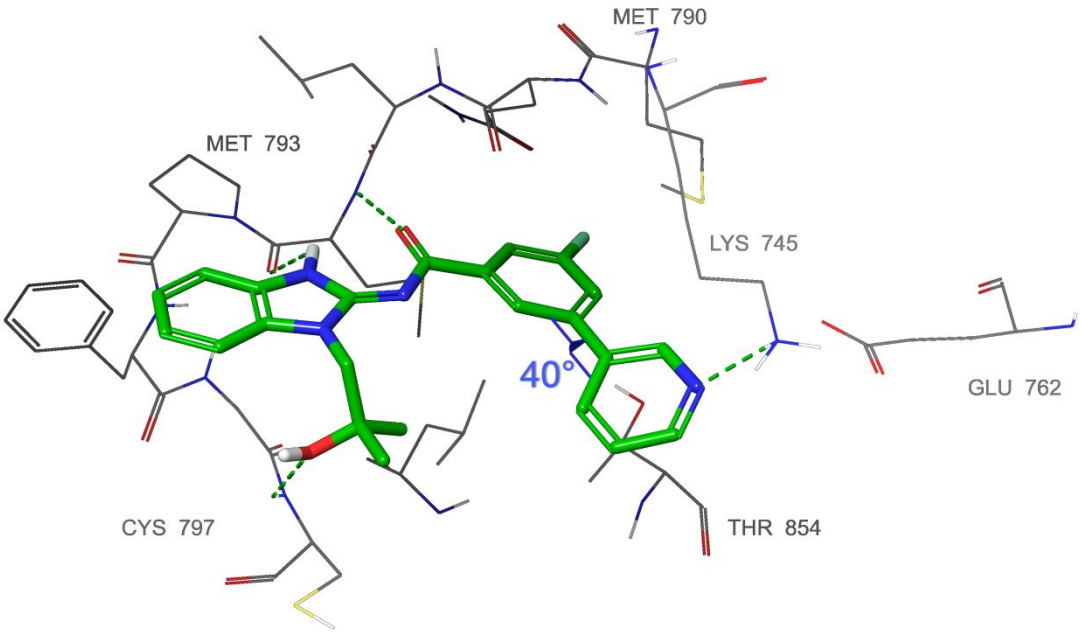

Figure 3. X-ray structure of ligand **1** (PDB: 6S9B) bound to the ATP pocket of the $EGFR^{L858R\ T790M}$ protein.

EGFR^{L858R} protein was used for protein crystallography as EGFR^{del19} protein has proven particularly recalcitrant to x-ray crystallography with no structures published. Compound **1** was successfully crystallized with EGFR^{L858R} with the gatekeeper mutation T790M (**Figure 3**). From the x-ray structure a two-point hinge binding motive can be seen, with the benzimidazole N-H and carbonyl group binding to Met793. The isobutyl hydroxy group fills the sugar pocket[51] of the kinase while the pyridine substituent in R_2-position (nomenclature see **Figure 4**) binds to the Lys745 in the phosphate region of the pocket. No clash between the bulky Met790 gatekeeper residue and the benzimidazole is observed. Important for our further optimization was the observation that the torsion angle between the two aromatic rings of **1** is ~40°, which was found to be a low energy conformation based on a QM-torsion angle scan (see **Figure 4**). Therefore, the dihedral angle was scanned in 10° steps while optimizing all other degrees of freedom within the ligand on ωB97XD/cc-pVDZ level of theory.[52]

A close analog (**2**) missing the fluorine atom in the R_1 position (see **Table 1**) was found to show a similar activities in the biochemical and biomarker assays (IC_{50} EGFR$^{L858R\ T790M\ C797S}$ = 2,700 nM; IC_{50} EGFR$^{del19\ T790M\ C797S}$ = 173 nM). Due to synthetic accessibility, we

decided to move on with our further optimization program without a substituent in the R_1 position.

In the next step, we decided to address the hydroxyl group of the side chain of Thr854 via a nitrogen acceptor from the X-position of the central aromatic ring system (see **Figure 4**). In addition, the newly designed ligands should still have a torsion angle of 30-40° at a low energy conformation to enable a proper interaction with Lys754. In order to access both requirements we performed a QM-torsion angle scan for the bis aryl system of the newly designed compounds **3**, **3a** and **4** (**Figure 4**).

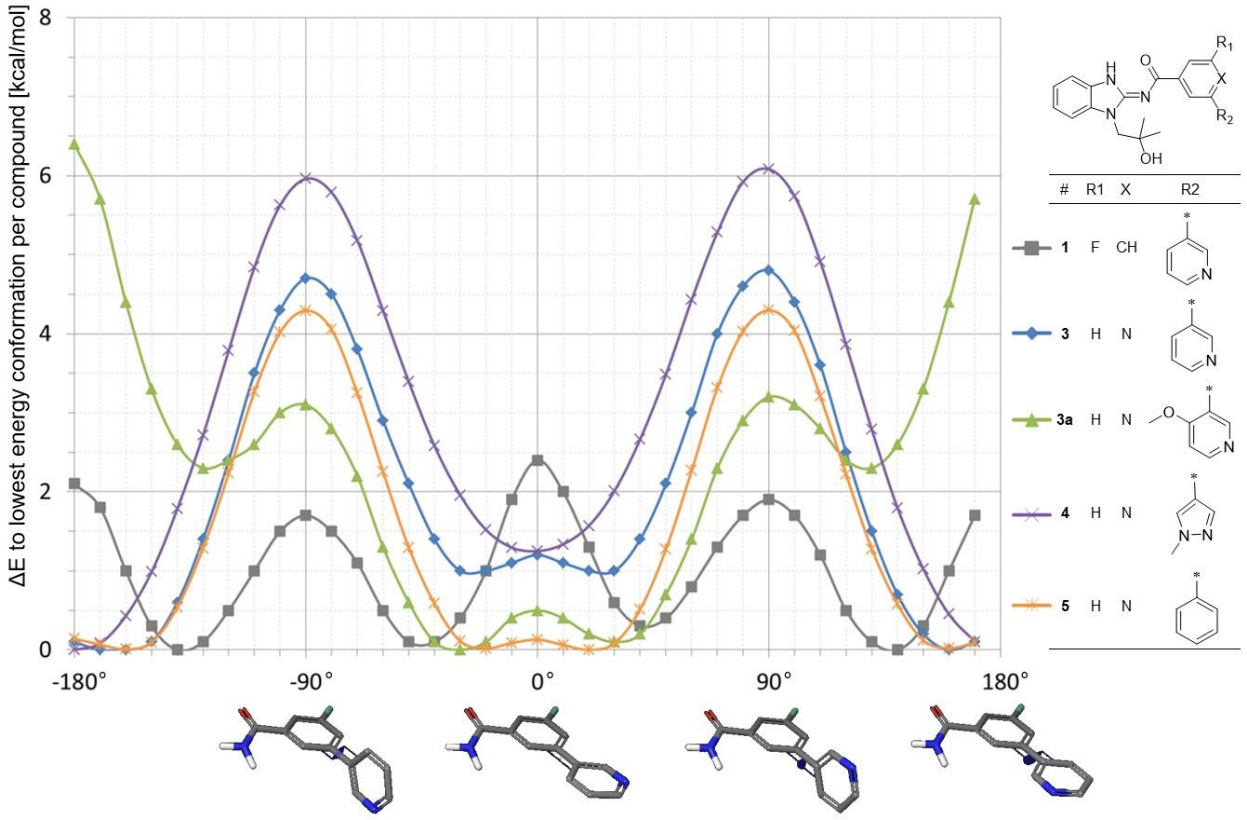

Figure 4. QM-torsion angle scans for compounds **1**, **3**, **3a**, **4** and **5**. The baseline energy is set for each compound individually (to zero), and not deducted from the lowest energy of all compounds.

The pyridyl nitrogen of the R_2 moiety of compound **3** de-symmetrizes the bis aryl system further and therefore a lager energy difference between the minima (30° and 160°) in comparison to compound **1** is observed (see **Figure 4**). In case of the minimum at 30°, both pyridyl nitrogens of compound **3** are located at the same side, which leads to an unfavorable dipole-dipole interaction (overall dipole: 3.87 Debye) compared to the

minimum at 160° for which the pyridyl nitrogens are located at the opposite side leading to partial dipole cancellation (overall dipole: 2.35 Debye).

The local minimum at 30° of compound **3** would allow the ligand to interact via the pyridyl nitrogen of the R_2 moiety with Lys745. However, this local minimum is approximately 1 kcal/mol higher than the absolute minimum, which is located at 160°. Therefore, an energy penalty has to be paid for the non-optimal dihedral angle, but a gain in binding affinity was expected due to the interaction with Thr854. Interestingly, the benzimidazole **3** showed a factor of 3-8 improved activity in the biochemical assays (IC_{50} $EGFR^{L858R\ T790M\ C797S}$ = 353 nM; IC_{50} $EGFR^{del19\ T790M\ C797S}$ = 57 nM) and demonstrated an even more pronounced gain in potency in the cellular biomarker modulation assay, while at the same time maintaining the low affinity for wild type EGFR.

For compound **4** a similar situation was observed. A local minimum was found at a torsion angle of 0°, while the absolute minimum is approximately 1 kcal/mol lower and is located at 180°. Again, an energy penalty must be paid for the non-optimal dihedral angle, but on the other hand a gain in binding affinity could be expected due to the interaction with Thr854. Also, for compound **4** a slight improvement of activity was observed in

biochemical and an even more pronounced gain in the cellular biomarker modulation assay.

We investigated several different aromatic ring systems for the R_2 position with the goal to identify motifs, which would bind with the absolute minimum conformation regarding the dihedral angle of the bis aryl system to EGFR. One possible solution is shown by compound **3a**, which bears a 4-methoxy-pyrid-3-yl moiety at the R_2 position. The QM-torsion angle scan (see **Figure 4**) for the bis aryl system showed high energy for dihedral angle 160-180° due to unfavorable interactions of the methoxy group and the facing pyridyl nitrogen, but an absolute minimum at 30°. The unfavorable dipole-dipole interaction between the two ring nitrogen atoms at 30° is also given for compound **3a**, but the energy penalty is compensated by the favorable electrostatic interactions of the methoxy group with the facing proton (see **Supplementary Figure 1**). Therefore the energy at 30° of ligand **3a** is lower than for compound **3**. This optimized binding conformation of ligand **3a** translates in a 30-fold improved biochemical activity based of the $EGFR^{L858R\ T790M\ C797S}$ protein compared to ligand **3** and **4**. The same trend can be seen comparing the biochemical $EGFR^{del19\ T790M\ C797S}$ data. This improved biochemical activity lead to a

35-fold improved p-EGFR$^{del19\ T790M\ C797S}$ biomarker modulation and in a 5-fold improved anti-proliferative effect in BaF3 cells compared to ligand **3** and **4**. However, the compound displayed a clearly lower general kinase selectivity compared to compound **3** and **4** (36% hits; see **Table 1**). These data show that activity can be massively gained by optimal interaction with Lys745, but at the expense of reduced kinase selectivity.

We hypothesized, that better kinase selectivity could be achieved, if the pocket around Lys745 (phosphate region) is addressed by an aromatic system which bears no acceptor. Prerequisite for this strategy was that the envisioned R_2 moiety does not clash with Lys745, which could be achieved with a dihedral angle of <20°.

To probe the hypothesis, we synthesized benzimidazole **5**, which does not contain a hydrogen bond acceptor atom in the second aromatic ring and carries only a symmetric phenyl ring in the R_2-position. Therefore almost no energy difference is seen between the minima (20° and 160°; see **Figure 4**). To our delight, we found that, while the biochemical and cellular potency against EGFR mutated cells was basically unchanged compared to compound **3**, the selectivity was significantly improved, as it is evident from the not observable cytotoxic activity against EGFR independent cells. At the same time,

the kinase selectivity was found to be very high, as only mutant EGFR was hit amongst a panel of 30 kinases. Furthermore, benzimidazole **5** also showed an excellent wt-sparing effect based on the comparison of the anti-proliferative effect on $EGFR^{del19\ T790M\ C797S}$ versus $EGFR^{wt}$ in BaF3 cell lines (see **Table 1**).

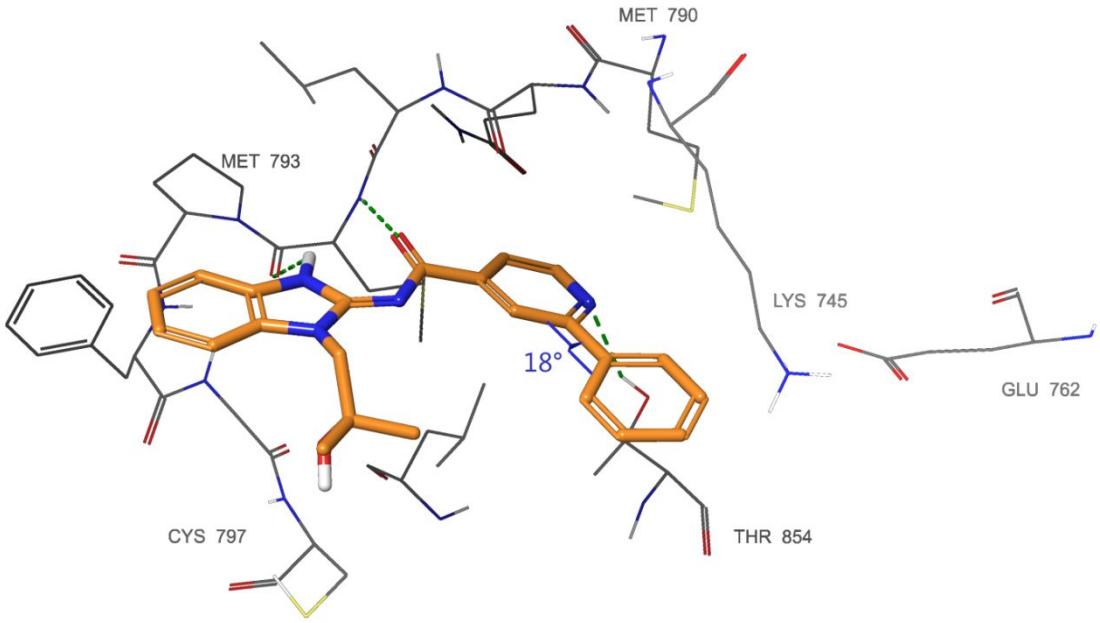

Figure 5. X-ray structure of compound **5** (PDB: 6S9C) in complex with $EGFR^{L858R\ T790M}$.

The x-ray structure of compound **5** with $EGFR^{L858R\ T790M}$ shows (see **Figure 5**), that the compound binds to the protein with the expected dihedral angle of the bis aryl system of approximately 20°. In addition, the distance to the Lys745 and Glu762 is sufficiently large (3.5 Å) to avoid a clash.

Table 1. SAR for the open-chain aminobenzimidazoles **1**-**5**.

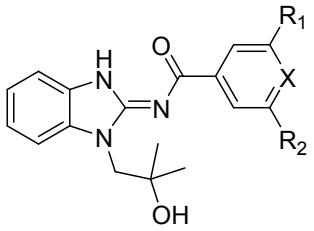

#	R_1	X	R_2	Biochemical kinase assays[a]: IC_{50} [nM] EGFR$^{d19\ TM\ CS*}$	EGFR$^{LR\ TM\ CS**}$	EGFR^{wt}	Kinase sel.[b]: %hit (#total) @ 1 µM	BaF3 cells biom.[c]: IC_{50} [nM] p-EGFR$^{d19\ TM\ CS*}$	BaF3 cells anit-proliferation[d]: IC_{50} [nM] EGFR$^{d19\ TM\ CS*}$	EGFR^{wt}	EGFR indep.
1	F	CH	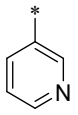	250 (1.13)	2,100 (1.08)	>100,000	3% (30) 5% (238)	790 (1.09)	nd	nd	nd
2	H	CH	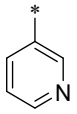	173 (1.17)	2,700 (1.38)	>100,000	13% (30)	1,400 (1.32)	nd	nd	nd
3	H	N	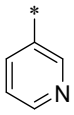	57 (1.13)	353 (1.42)	>100,000	10% (30) 11% (238)	35 (1.27)	270 (1.21)	3,600 (1.22)	3,500 (1.35)
3a	H	N	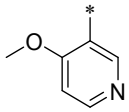	≤ 3[#]	12 (1.07)	10,000	36% (30)	1.0 (1.08)	51 (1.18)	700 (1.04)	990 (1.06)
4	H	N	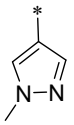	72 (1.12)	519 (1.14)	>100,000	10% (30)	43 (1.56)	333 (1.24)	5,100 (1.45)	8,900 (1.12)
5	H	N	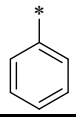	35 (1.15)	267 (1.18)	>100,000	0% (30)	22 (1.27)	150 (1.29)	>10,000	>25,000

Data are reported as geometric mean of at least 3 independent measurements and in brackets is the geometric standard deviation as multiplicative factor given; [a] biochemical kinase assay using different EGFR variants, which measures the inhibitory effect of compounds on the phosphorylation activity of EGFR enzyme forms on poly-GT substrate in the presence of ATP; [b] kinase selectivity was determined using the "SelectScreen Kinase Profiling Services" from ThermoFisher; [c] measurement of inhibition of the p-EGFR$^{del19\ T790M\ C797S}$ signal in BaF3 cells after 4 h compound treatment; [d]BaF3 cells bearing EGFR$^{del19\ T790M\ C797S}$ protein were treated for 3 days with compound, the effect on

proliferation was measured; nd means not determined; *$EGFR^{d19\ TM\ CS}$ means $EGFR^{del19\ T790M\ C797S}$; **$EGFRLR^{\ TM\ CS}$ means $EGFR^{\ L858R\ T790M\ C797S}$; #activity of compound at or below assay wall (assay wall around 3 nM due to enzyme concentration/activity and substrate concentration).

Entropy driven optimization: Rigidification through macrocyclization

Compound **5** represented a selective but not yet sufficiently potent compound (**Table 1**, Entry 6). In analogy to the discovery of lorlatinib,[11] we chose reduction of ligand entropy through macrocyclization as the strategy to improve potency.[53-55] We pursued both theoretical and experimental methods to assist the design of cyclized compounds. Initially, as for the computational conformation analysis of ligand **5,** the MOE module LowModeMD[56], followed by semi empirical (MOPAC, AM1) energy minimization of all the conformers *in vacuo* was employed for the analysis and selection of low-energy conformers. In the course of the project, we then complemented this approach with enhanced sampling molecular dynamics methods in explicit solvation[57]. These findings were supported by a detailed 2D NMR analysis of compound **5** which showed ROE correlations between protons, as indicated in **Scheme 1**. The ROEs support the presence

of both active and inactive conformational states in the population observed in solution. This was further corroborated by QM-DFT ^{13}C, ^{1}H and partial ^{15}N chemical shift predictions which support a Boltzmann-weighted energy distribution, with significant population of active and inactive conformers.[57, 58] We therefore expected a significant improvement of binding affinity to $EGFR^{del19\ T790M\ C979S}$ if the molecule could be constrained in its “active” binding conformation.

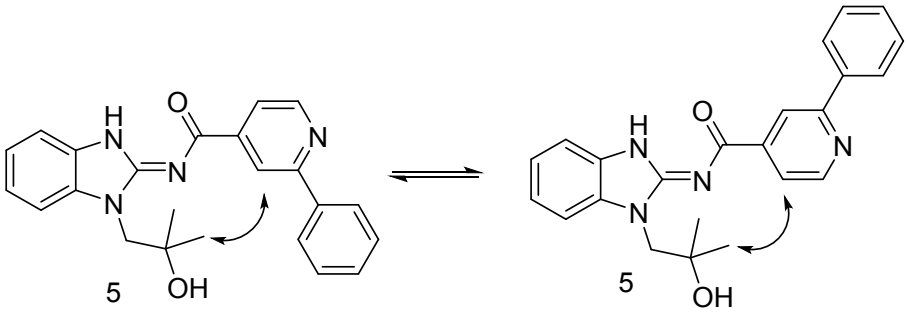

Scheme 1. 2-Dimensional representation of the most prevalent conformations of ligand **5** as computationally predicted and detected in solution by 2D-NMR. Important ROE-correlations are displayed as arrows.

Starting from ligand **5** as a template for the active conformation, several different macrocyclic variants with varying linker lengths and attachment points were designed. The macrocycles were then virtually subjected to conformational searches (MOE

LowModeMD),[56] followed by AM1 energy minimization of all conformers. Low energy conformations were compared with the binding conformation of amino benzimidazole **5** and macrocyclic ligand **6**, with a $C_5H_{10}O$ linker was found to display a good overlap with the desired "active" conformation (see **Figure 6**).

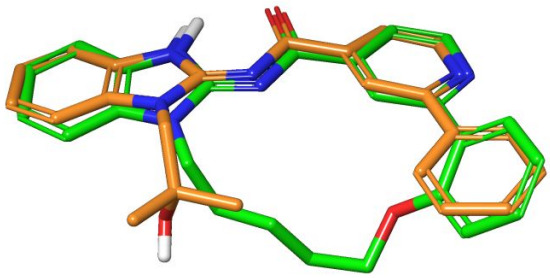

Figure 6. Overlay of x-ray-based structure of compound **5** (orange) and calculated minimum conformation structure of macrocyclic ligand **6** (green).

The first macrocyclic ligand **6** displayed a biochemical activity in the $EGFR^{del19\ T790M\ C797S}$ assay at the assay wall[58], which hampers the evaluation of the activity improvement. Fortunately, the biochemical activity of macrocycle **6** in the $EGFR^{L858R\ T790M\ C797S}$ assay is still above the assay wall (see **Supplementary Table 8**, entry 1) and therefore a 17 fold improved biochemical activity over the open chain ligand **5** can be determined. The gain

in biochemical activity translates in a 5-fold improvement of cellular potency over the open chain ligand **5** as is evident from the inhibition of the p-EGFR signal and antiproliferative effect on $EGFR^{del19\ T790M\ C979S}$ dependent BaF3 cells (see **Table 2**, entry 1). Noteworthy for compound **6** was a favorable $EGFR^{wt}$ and general kinase selectivity (0/30 kinases were hit @ 1μM)[50] observed.

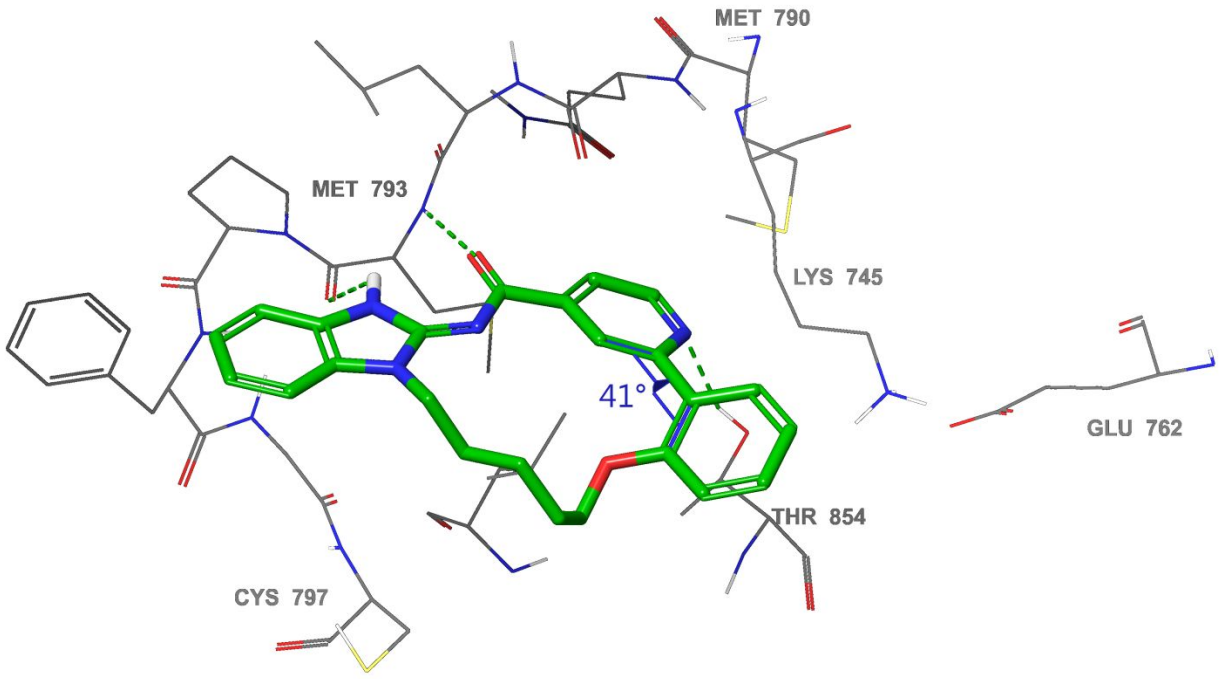

Figure 7. X-ray structure of compound **6** (PDB: 6S9D) in complex with $EGFR^{L85R\ T790M}$.

From the protein x-ray structure (see **Figure 7**), it is evident that the observed potency improvement resulted mostly from the conformational restrictions as no new or changed

interactions with the EGFR protein are visible. Also, the observed binding conformation of ligand **6** is in excellent agreement with the computationally predicted minimum conformation.

From the predicted minimum energy conformation of ligand **6** it was expected that the bis aryl torsion angle in the macrocyclic ligand should be constrained to approx.~40°, a value which is very close to the observed angle in the x-ray structure (39°) (see **Figure 7**). This indicated that a re-installment of a hydrogen bond acceptor in the second aromatic ring should lead to a favorable hydrogen bond formation to Lys745. Therefore, we decided to further improve the potency of the molecule by implementing a polar interaction with Lys745, as it was seen in ligands **1**-**4**. We chose the *N*-methylpyrazole from ligand **4** rather than the pyridine moiety of compound **3**, because the metabolic stability predicted from human hepatocytes was superior for ligand **4** (%QH: 12%) over ligand **3** (%QH: 34%). Additionally, a fluorine atom was reinstalled in the α-position (R_1) of the pyridine nitrogen to fill the observed small sub-pocket in the protein x-ray structure of **6** with the EGFR protein (see **Figure 7**). We hypothesized that this substituent might

be in part responsible for the excellent general kinase selectivity of ligand **1**. These structural changes resulted in ligand **7**, which showed at least an additional 5-fold improved biochemical activity in the $EGFR^{L858R\ T790M\ C797S}$ assay. It is noteworthy that macrocycle **7** also shows activity around the assay wall in this biochemical assay (see **Supplementary Table 8**, entry 2). This prevents the use of biochemical EGFR assays to determine further potency improvements. Also, a 5-fold improved antiproliferative effect against $EGFR^{del19\ T790M\ C797S}$ dependent cells of ligand 7 versus 6 can be seen. At the same time, we observed a sub-micromolar antiproliferative effect against $EGFR^{wt}$ and EGFR independent cells for the first time. However, the ratio of the IC_{50} values remained unchanged between ligand **6** (IC_{50} $EGFR^{wt}$ / IC_{50} $EGFR^{del19\ T790M\ C797S}$ = 48) and ligand **7** (IC_{50} $EGFR^{wt}$ / IC_{50} $EGFR^{del19\ T790M\ C797S}$ = 45) suggesting a generally improved kinase activity instead of a specific improvement for mutant EGFR. The size of the substituent at the R_1-position was increased from fluorine to methyl which gave rise to compound **8.** While the cellular potency of aminobenzimidazole **8** (IC_{50} $EGFR^{del19\ T790M\ C797S}$ = 5 nM) was found to be unchanged compared to ligand **7** (IC_{50} $EGFR^{del19\ T790M\ C797S}$ = 6 nM), the selectivity for EGFR mutant dependent cells over $EGFR^{wt}$ dependent cell or EGFR

independent cells was significantly improved for ligand **8** (IC_{50} $EGFR^{wt}$ / IC_{50} $EGFR^{del19\ T790M\ C797S}$ = 460). The enhanced selectivity for EGFR mutant dependent cells over EGFR independent cells was also reflected by the improved overall kinase selectivity profile (see **Table 2**). For all further studies we kept the methyl group in the R_1-position as a "selectivity trigger", which allowed us to further improve the potency while maintaining excellent kinase selectivity.

In the next step we reinvestigated the 3-dimensional shape of our molecule by means of computational conformation analysis. From our previous computations and from the protein x-ray structures with ligand **6** we knew that the conformation of the macrocyclic ligands was not flat but rather bowl shaped. From the lack of a stereo center in the ligands **6**-**8** these bowl-shaped molecules could adopt two enantiotopic minimum energy conformations (see **Figure 8**: green and magenta ligand). We hypothesized that the interconversion between these two enantiotopic conformers would go through a low energy transition state and would be fast at room temperature. From the protein x-ray structures with ligand **6** the desired enantiomer was already known (see **Figure 7** and

Figure 8; green ligand), and we envisioned a further improvement of the cellular potency by an additional restriction of the ligand to only one enantiotopic minimum conformer. To do so, we decided to install a stereo center in the linker and therefore to de-symmetrize the molecule, so that the conformation at the newly installed stereo center would determine the conformational outcome of the entire ligand. Furthermore, we speculated that a correctly placed alkyl substituent in the linker would help to fill the "sugar-pocket" of the EGFR protein, which was previously filled by the bulky isobutyl-hydroxy group in the ligands **1**-**5**.

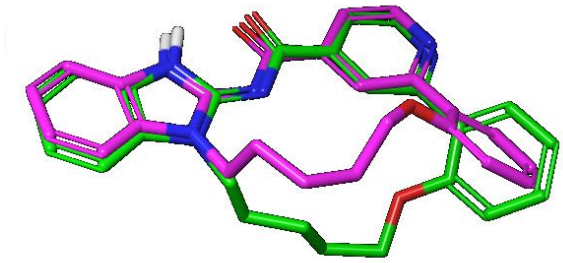

Figure 8. Two calculated enantiotopic minimum energy conformations of compound **6.**

Again, we compared the calculated minimum conformations of the newly designed ligands with the desired "active" conformation of ligand **6**, this time focusing our attention

towards the optimal conformation of the linker and the absolute configuration of the minimum conformers. After investigating numerous possible macrocyclic ligands, we decided to synthesize ligand **9** with an additional methyl group in 2-position of the linker. Based on our calculations, the newly installed stereogenic center needed to be (*R*)-configured to give the ligand in the desired shape. Satisfyingly, we found that ligand **9** shows an additional improvement in cellular potency against mutant EGFR dependent cells (IC_{50} $EGFR^{del19\ T790M\ C979S}$ = 1 nM) without losing the favorable selectivity window against $EGFR^{wt}$ dependent cell lines (IC_{50} $EGFR^{wt}$ / IC_{50} $EGFR^{del19\ T790M\ C979S}$ > 1,000) and EGFR independent cell lines, and as before the overall kinase selectivity was maintained. While we were unsuccessful in obtaining an x-ray crystal structure of this molecule with the EGFR protein, we were able to solve a small molecule x-ray structure of a very close analog of **9** bearing a bromine substituent at the R_3 position **9-Br** (see **Figure 9**)

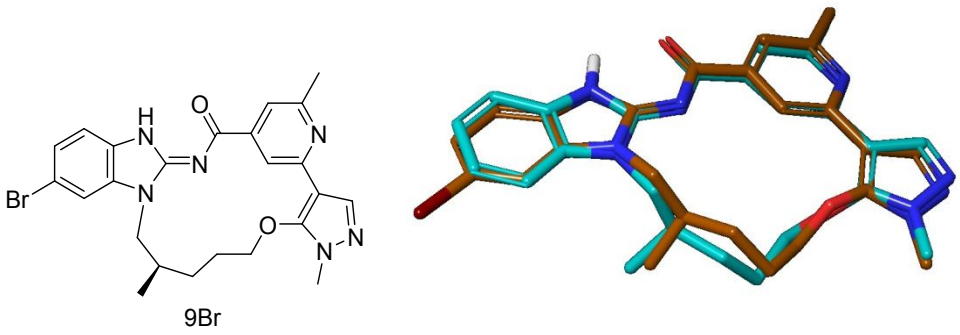

Figure 9. Structure of **9Br** and comparison of small compound x-ray structure of **9Br** (brown, CCDC 1941612) with the calculated minimum energy conformation of **9** (cyan).

The small molecule x-ray structure of **9Br** with the heavy atom in 6-position of the benzimidazole allowed not only for the unambiguous determination of the absolute configuration at the newly created stereo center (*R*-configuration) but also confirmed the predicted minimum energy conformation of **9** (see **Figure 9**).

At this point in the project we felt that no further optimization of the cellular potency of the benzimidazole ligands was necessary. Instead, we focused any further optimization towards improving the DMPK parameters of the molecules. Particularly, the high plasma protein binding and the low aqueous solubility of ligand **9** were of concern (see **Table 3**). We believed that the high lipophilicity at the phenyl core caused the observed low solubility. Therefore, we decided to investigate several different solubilizing groups

attached to the phenyl core. From the x-ray structure of ligand **6** (see **Figure 7**) with the EGFR protein, an exit vector towards the solvent from positions 5 and 6 of the benzimidazole core became apparent.

Table 2. SAR for the macrocyclic benzimidazoles **6** – **9** and **BI-4020**.

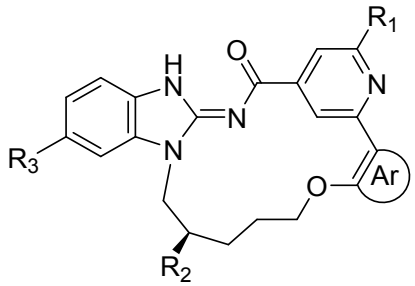

#	R_1	Ar	R_2	R_3	BaF3 cells biomarker[c]: IC_{50} [nM] p-EGFR$^{d19\ TM\ CS*}$	BaF3 cells anit-proliferation[d]: IC_{50} [nM] EGFR$^{d19\ TM\ CS*}$	EGFR^{wt}	EGFR indep.	Kinase sel.[b]: %hit (#total)
6	H		H	H	3.0 (1.10)	27 (1.10)	1,300 (1.13)	1,600 (1.17)	0% (30)
7	F	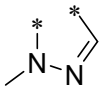	H	H	1.2 (1.11)	6.0 (1.42)	270 (1.10)	330 (1.24)	26% (30)
8	Me	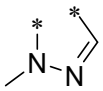	H	H	1.0 (1.10)	5.0 (1.15)	2,300 (1.21)	1,700 (1.22)	10% (30)
9	Me	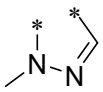	Me	H	0.8 (1.14)	1.0 (1.25)	1,100 (1.10)	1,000 (1.23)	13% (30)
BI-4020	Me	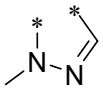	Me	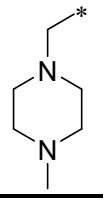	0.6 (1.07)	0.2 (1.15)	190 (1.19)	1,100 (1.15)	7% (30) 8% (238) 7% (393)

Data are reported as geometric mean of at least 3 independent measurements and in brackets is the geometric standard deviation as multiplicative factor given; [b] kinase selectivity was determined using the "SelectScreen Kinase Profiling Services" from ThermoFisher; [c] measurement of inhibition of the p- EGFR$^{del19\ T790M\ C797S}$ signal in BaF3 cells after 4 h compound treatment; [d]BaF3 cells bearing EGFR$^{del19\ T790M\ C797S}$ protein were treated for 3 days with compound, the effect on proliferation was measured; *EGFR$^{d19\ TM\ CS}$ means EGFR$^{del19\ T790M\ C797S}$

During our studies, we found that only very few substituents at the 5-position were accepted without dramatic loss in cellular activity (data not shown). Therefore, we decided to focus on solubilizing groups at the 6-position of the molecule and synthesized several ligands with varying solubilizing groups. From this collection of molecules ligand **BI-4020** was identified as the most promising ligand with optimally balanced properties. The human clearance predicted by hepatocytes of compound **BI-4020** was higher than for ligand **9**, but still in an acceptable range. Solubility, fraction unbound in plasma and permeability of ligand **BI-4020** were clearly improved compared to ligand **9**.

Surprisingly, an additional boost in cellular activity was observed with ligand **BI-4020** (IC_{50} $EGFR^{del19\ T790M\ C979S}$ = 0.2 nM) showing for the first time sub-nanomolar activity. Pampa data indicate, that the cellular potency gain could be explained by the improved permeability of BI-4020 (Papp A-B @ pH 7.4: 5.3×10^{-6} cm/s) compared to ligand **9** (Papp A-B @ pH 7.4: 0.2×10^{-6} cm/s). While the absolute activity on $EGFR^{wt}$ was also significantly increased (IC_{50} $EGFR^{wt}$ = 190 nM) the ratio between $EGFR^{wt}$ and EGFR mutant dependent cells remained high (IC_{50} $EGFR^{wt}$ / IC_{50} $EGFR^{del19\ T790M\ C979S}$ > 950).

Furthermore, the ratio between EGFR independent and EGFR mutant dependent cells was even increased. The kinase selectivity, now measured on three different panels (30 kinases, 238 kinases and 394 kinases), remained also unchanged.

Table 3. DMPK properties of macrocycle **9** and **BI-4020** in comparison to osimertinib.

#	Solubility[a] @ pH 6.8 [µg/ml]	Metabolic stability Hepatocytes[b] [%QH] Mouse	Human	PPB free fraction[c] Mouse	Human	Permeability Pampa assay[d] Papp A-B [cm/s] @ pH 7.4
9	< 0.1	47	12	<0.3	0.5	$0.2x10^{-6}$
BI-4020	95	56	47	1.2	7.5	$5.3x10^{-6}$
Osimertinib	86	83	27	<0.1	2.5	$2.7x10^{-6}$

[a] Aqueous solubility were determined from 1 mg/mL solid compound dispensed into aqueous McIlvaine buffer (pH 6.8); [b] In-vivo hepatic clearance (CL) was predicted by in-vitro incubations of 1 µM EGFR TKI with cryopreserved hepatocytes (Celsis IVT) and measured depletion over 240 minutes by quantitation of EGFR TKI by LC/MS/MS; [c] Plasma protein binding (PPB) was determined by equilibrium dialysis. Plasma was spiked with EGFR TKI and dialyzed against Soerensen buffer (pH 7.4) for 3 hours at 37°C; [d] permeability was accessed by using a chamber separated by a microfilter disc (coated with structured layers of immobilized artificial phospholipid membranes) into a donor and an acceptor area.

Aqueous solubility were determined from 1 mg/mL solid compound dispensed into aqueous McIlvaine buffer (pH 4.5 or 6.8), or dissolved in acetonitrile/water (1:1) as reference. Dissolved concentrations were determined with an Agilent 1200 HPLC/DAD-UV system.

Plasma protein binding (PPB) was determined by equilibrium dialysis. Plasma was spiked with EGFR TKI and dialyzed against Soerensen buffer (pH 7.4) for 3 hours at 37°C. PPB was calculated by quantifying EGFR TKI concentrations in plasma and buffer by HPLC/MS-MS. *In-vivo* hepatic clearance (CL) was predicted by *in-vitro* incubations of EGFR TKI with cryopreserved hepatocytes (Celsis IVT) and measured depletion over 240 minutes by quantitation of EGFR TKI by LC/MS/MS and using the well-stirred model. PAMPA parameters were determined as described previously.[65]

Next, we benchmarked the antiproliferative effects of **BI-4020** with osimertinib in a series of relevant EGFR mutant cell lines (see **Table 4**).

Table 4. Comparison between ligand **BI-4020** and **osimertinib.**

Cellular potency[d]	Unit	**BI-4020**	**Osimertinib**
IC_{50} p-EGFR BaF3 ($EGFR^{del19TMCS*}$)	[nM]	0.6 (1.07)	3100 (1.22)
IC_{50} BaF3 ($EGFR^{del19TMCS*}$)	[nM]	0.2 (1.15)	780 (1.06)
IC_{50} BaF3 ($EGFR^{del19}$)	[nM]	1 (1.09)	1 (1.11)
IC_{50} BaF3 ($EGFR^{wt}$)	[nM]	190 (1.19)	81 (1.16)
IC_{50} BaF3 (EGFR indep.)	[nM]	1100 (1.15)	1100 (1.23)
IC_{50} PC-9 ($EGFR^{del19TMCS*}$)	[nM]	1.3 (1.10)	>1,000
IC_{50} A431 ($EGFR^{wt}$)	[nM]	200 (1.12)	84 (1.05)
Kinase Selectivity[b]	%hit (#total)	8% (238)	7% (238)

Data are reported as geometric mean of at least 3 independent measurements and in brackets is the geometric standard deviation as multiplicative factor given; [d]BaF3 cells bearing different EGFR variants were treated for 3 days with compound, the effect on proliferation was measured; *$EGFR^{del19\ TM\ CS}$ means $EGFR^{del19\ T790M\ C797S}$

While the covalent inhibitor osimertinib showed only weak in vitro biomarker modulation of the triple mutant EGFR due to the Cys797 to Ser797 resistance mutation, non-covalent inhibitor **BI-4020** showed strong sub-nanomolar potency (see **Table 4**). The strong biomarker modulation of ligand **BI-4020** translates into sub-nanomolar antiproliferative effects against $EGFR^{del19\ T790M\ C979S}$ dependent BaF3 cells, whereas osimertinib was approximately 4000-fold less active. Osimertinib and **BI-4020** display equivalent activity

on $EGFR^{del19}$ BaF3 cells as well as comparable selectivity for EGFR mutant over $EGFR^{wt}$ (see **Table 4**). As expected already from the BaF3 cell profile also an excellent potency of 1.3 nM was observed for **BI-4020** in the NSCLC cell line PC-$9^{del19\ T790M\ C797S}$, whereas osimertinib shows no anti proliferative effect up to 1 µM. The great EGFR wt-sparing effect of BI-4020 (150 fold; see **Table 4**) could be also demonstrated using the NSCLC cell pair A431 ($EGFR^{wt}$) and PC-$9^{del19\ T790M\ C797S}$.

In-vitro and In-vivo characterization of macrocycle **BI-4020***: first EGFR TKI showing regression in an EGFR$^{del19\ T790M\ C797S}$ model*

Based on the high potency and favorable *in-vitro* DMPK parameters (see **Table 3** and **Table 4**) the macrocycle **BI-4020** was chosen for *in-vivo* studies. The measured clearance of 56 % QH nicely matches the predicted clearance from hepatocytes. A volume of distribution of 4.2 l/kg indicates good distribution into tissue. After oral dosing of 10 mg/kg a medium bioavailability is observed and the unbound IC_{50} is covered for more than 6 hours enabling further biomarker studies (see **Supplementary Figure 4**).

In order to test the ability of the macrocycle **BI-4020** to inhibit EGFR *in-vivo*, mice bearing subcutaneous PC-9$^{del19\ T790M\ C797S}$ xenotransplants were treated orally with the vehicle (natrosol) or 10 mg/kg of compound **BI-4020**. Tumors were subsequently harvested 6 h, 18 h and 24 h after treatment with **BI-4020**. Analysis and quantification of Tyr1068 phosphorylated EGFR (p-EGFR) from tumor lysates revealed that single oral administration of 10 mg/kg of **BI-4020** suppressed EGFR$^{del19\ T790M\ C797S}$ phosphorylation 5-fold to 10-fold at all three time points compared to the 6 h vehicle control (see **Figure**

10). These results demonstrate pharmacodynamic biomarker modulation of double resistance mutation-positive EGFR *in-vivo* by oral administration of compound **BI-4020** across a 24 h period and prompted us to conduct tumor growth efficacy experiments.

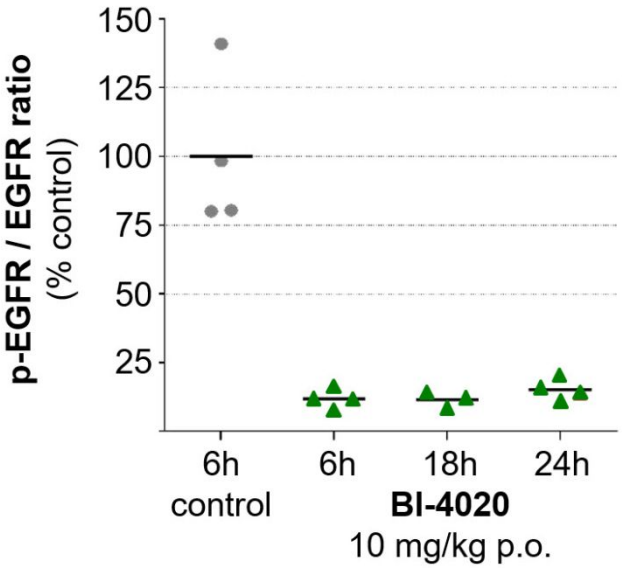

Figure 10. *In-vivo* biomarker modulation by macrocycle **BI-4020;** x-axis: time point of biomarker analysis after treatment with vehicle (control) or with 10 mg/kg BI-4020 p.o.; y-axis: ratio of p-EGFR signal versus EGFR total signal.

Daily oral treatment with 10 mg/kg **BI-4020** was tested for *in-vivo* efficacy in the *EGFR*$^{del19\ T790M\ C797S}$ mutant human non-small cell lung cancer model PC-9$^{del19\ T790M\ C797S}$. At treatment start the tumors displaying a size between 53 and 153 mm³. All groups were treated for 19 days. **BI-4020** induced strong regressions in 10 out of 10 tumors leading to

a TGI of 121 % (P = 0.0005) (see **Figure 11**), while daily treatment with 25 mg/kg osimertinib showed no effect of tumor growth with a TGI of 6 % in the same model (p>0.05). Both treatments were well tolerated in all mice.

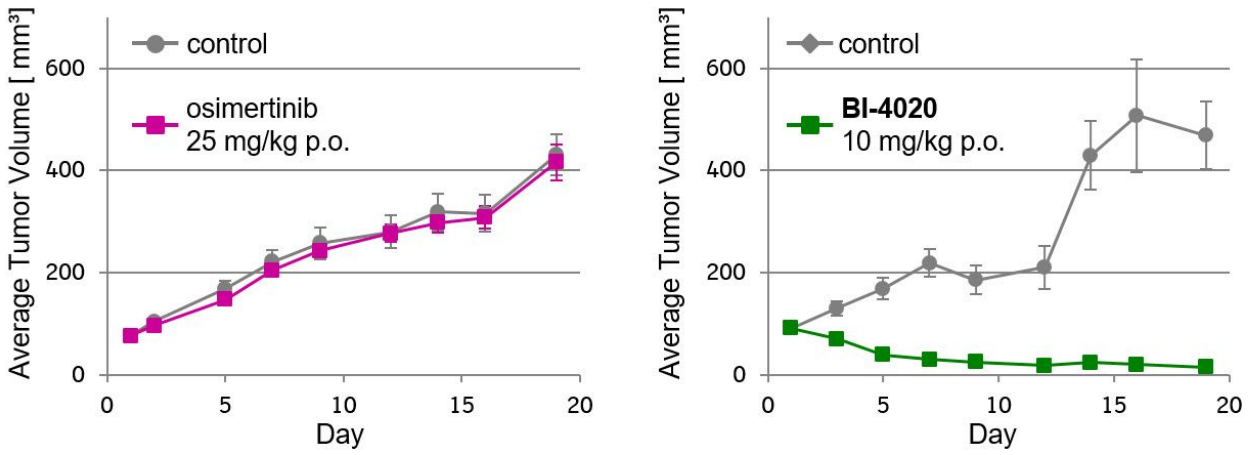

		Dose p.o. [mg/kg]	Schedule	TGI @ d19 [%]	p_{Value}	Mortality [x/10]
control		-	qd	-	*	0
osimertinib		25	qd	6	>0.05	0
BI-4020		10	qd	121	0.0005	0

Figure 11. Xenograft model with PC-9 cells bearing a $EGFR^{del19\ T790M\ C797S}$ protein; control group: 10 animals; treatment groups: 8 animals; animal type and strain: 6-8 week old, female BomTac:*NMRI-Foxn1*^{nu} mice.

SYNTHESIS

Schemes 2-7 illustrate the routes that were used to synthesize the compounds described herein.

Carboxylic acids **13a-f** were synthesized applying a Suzuki reaction of the commercially available bromides **11a-d** and boronic acids **12a-d** followed by an ester cleavage. Amide coupling of aminobenzimidazole **14** and carboxylic acids **13a-f** led to the final compounds **1-5** (see **Scheme 2**).

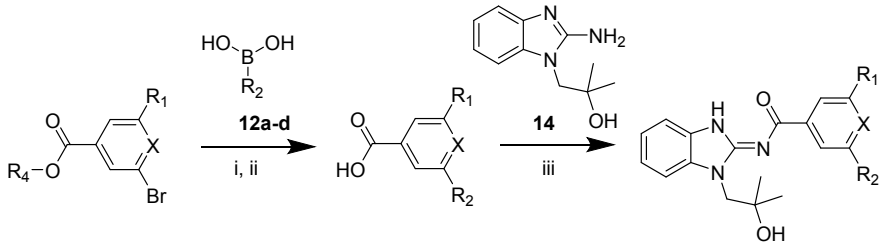

11

11a: R_1 = F; R_4 = H; X = CH;
11b: R_1 = H; R_4 = Me; X = CH;
11c: R_1 = H; R_4 = tBu; X = N;
11d: R_1 = H; R_4 = Me; X = N;

12a: R_2 = pyridine-3-yl
12b: R_2 = 4-Methoxy-pyridine-3-yl
12c: R_2 = 1-Methyl-1H-pyrazol-4-yl
12d: R_2 = phenyl

13a: R_1 = F; X = CH; R_2 = pyridine-3-yl
13b: R_1 = H; X = CH; R_2 = pyridine-3-yl
13c: R_1 = H; X = N; R_2 = pyridine-3-yl
13d: R_1 = H; X = N; R_2 = 4-Methoxy-pyridine-3-yl
13e: R_1 = H; X = N; R_2 = 1-Methyl-1H-pyrazol-4-yl
13f: R_1 = H; X = N; R_2 = phenyl

Scheme 2. Synthesis of compounds 1-5: Reagents and conditions: (i) Pd dppf, Cs_2CO_3, DME, water, 90 °C; 16 h; (ii) LiOH, THF, MeOH, 20 °C, 2 h; (iii) HATU, DIPEA, dioxane, 60 °C, 12 h.

Key intermediates **22a-c** were synthesized from starting material **15** applying an alkylation reaction followed by the reduction of the nitro group in intermediate **17** and a ring closure reaction of diamine **18**. Alternatively, key intermediates **22a-c** were synthesized by alkylating phenols **16b-c** with 1,5-dibromo-pentane **19** followed by a substitution reaction of **20a-b** with aminobenzimidazole **21**. Final compounds **6**, **7** and **9Br** were synthesized from **22a-c** by cleaving the ester followed by an amide coupling. Key intermediate **26** was synthesized from aminobenzimidazole **21** applying an alkylation reaction with bromide **23** followed by an amide coupling with carboxylic acid **25**. Final compound **8** was synthesized via a Mitsunobu reaction starting from intermediate **26** (see **Scheme 3**).

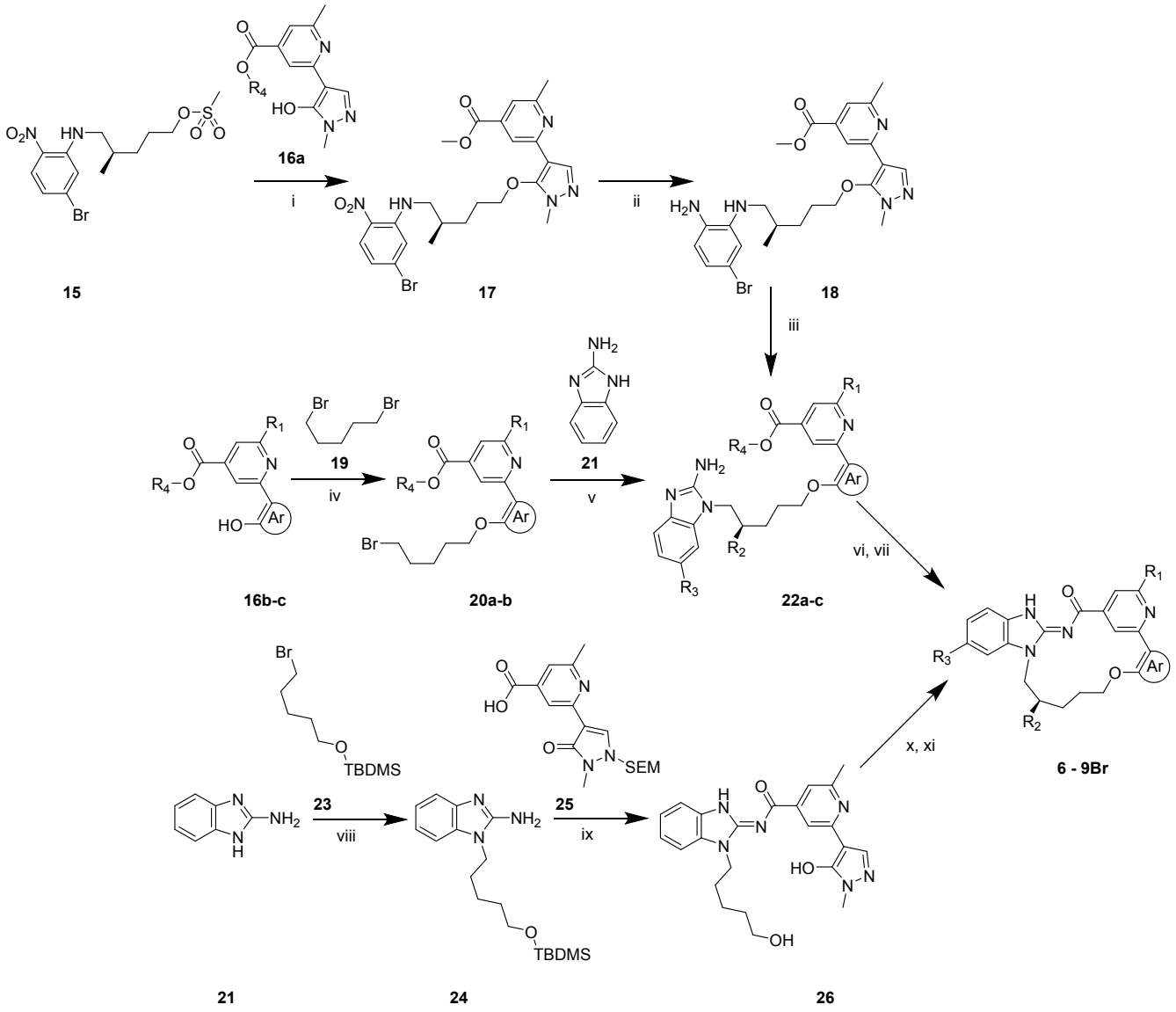

16a: R_1 = Me; Ar = methylpyrazol; R_4 = Me;
16b: R_1 = H; Ar = phenyl; R_4 = tBu;
16c: R_1 = F; Ar = methylpyrazol; R_4 = Me;

20a: R_1 = H; Ar = phenyl; R_4 = tBu;
20b: R_1 = F; Ar = methylpyrazol; R_4 = Me;

22a: R_1 = Me; R_2 = Me; Ar = methylpyrazol; R_3 = Br; R_4 = Me;
22a': R_1 = Me; R_2 = Me; Ar = methylpyrazol; R_3 = Br; R_4 = H;
22b: R_1 = H; R_2 = H; Ar = phenyl; R_3 = H; R_4 = tBu;
22c: R_1 = F; R_2 = H; Ar = methylpyrazol; R_3 = H; R_4 = H;

Scheme 3. Synthesis of compounds **6-9Br**: Reagents and conditions: (i) DMF, K_2CO_3, 60 °C, 16 h; (ii) Pt&V/C, 3 bar H_2, MeOH, 20 °C, 16 h; (iii) CN-Br, CH_2Cl_2, *t*-BuOH, 20 °C, 18 h; (iv) ACN, K_2CO_3, reflux, 16 h; (v) ACN, K_2CO_3, 110 °C (MW), 16 h; (vi) NaOH, THF, water, 20 °C, 1 h; (vii) TBTU, NEt_3, CH_2Cl_2, 20 °C, 30 min; (viii) ACN, K_2CO_3, reflux, 16 h; (ix) HATU, EtNi-Pr_2, dioxane, 20 °C, 16 h; (x) HCl in dioxane, EtOH, 20 °C, 16 h; (xi) PPh_3, DIAD, THF, 20 °C, 30 min.

Catalytic hydrogenation of **9Br** with palladium on carbon led to macrocycle **9**. Benzimidazol **BI-4020** was synthesized from key intermediate **9Br** applying a reductive carbonylation reaction, which led to aldehyde **27**, followed by a reductive amination reaction (see **Scheme 4**.)

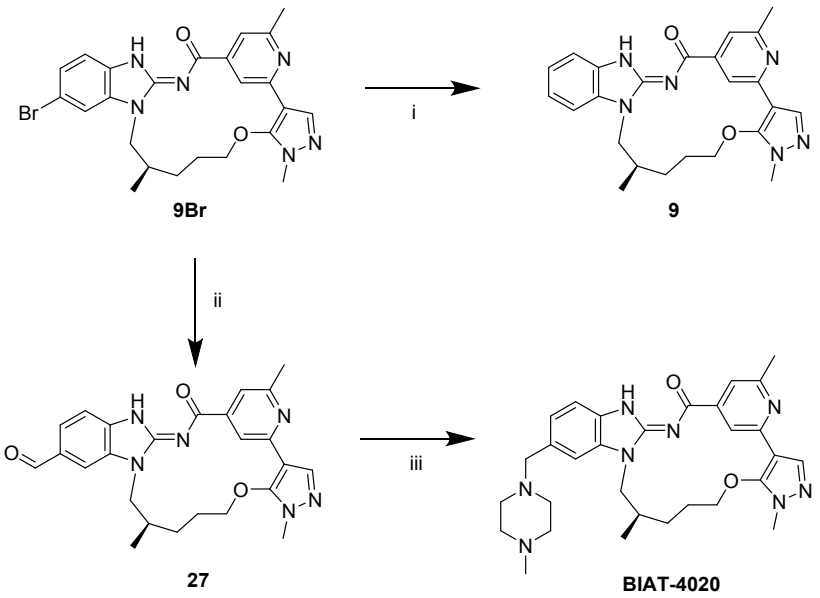

Scheme 4. Synthesis of compounds **9** and **BI-4020**: Reagents and conditions: (i) Pd/C, H_2, MeOH, 20 °C, 4 h; (ii) $Pd(OAc)_2$, Di(1-adamantyl)-n-butylphosphine, TMEDA, H_2/CO, dioxane, 100 °C, 24 h; (iii) $NaBH(OAc)_3$, HOAc, CH_2Cl_2, 20 °C, 6 h.

Phenols **16a** and **16b** were synthesized via a palladium catalyzed cross coupling reaction from chloropyridines **28** and **30**. Biaryl **36** was synthesized via Suzuki coupling of iodide **35** with boronic ester **34**, which was prepared by a CH activation of pyridine

derivate **32**. De-protection of phenolether **36** applying a palladium catalyzed debenzylation reaction led to phenol **16c** (see **Scheme 5**).

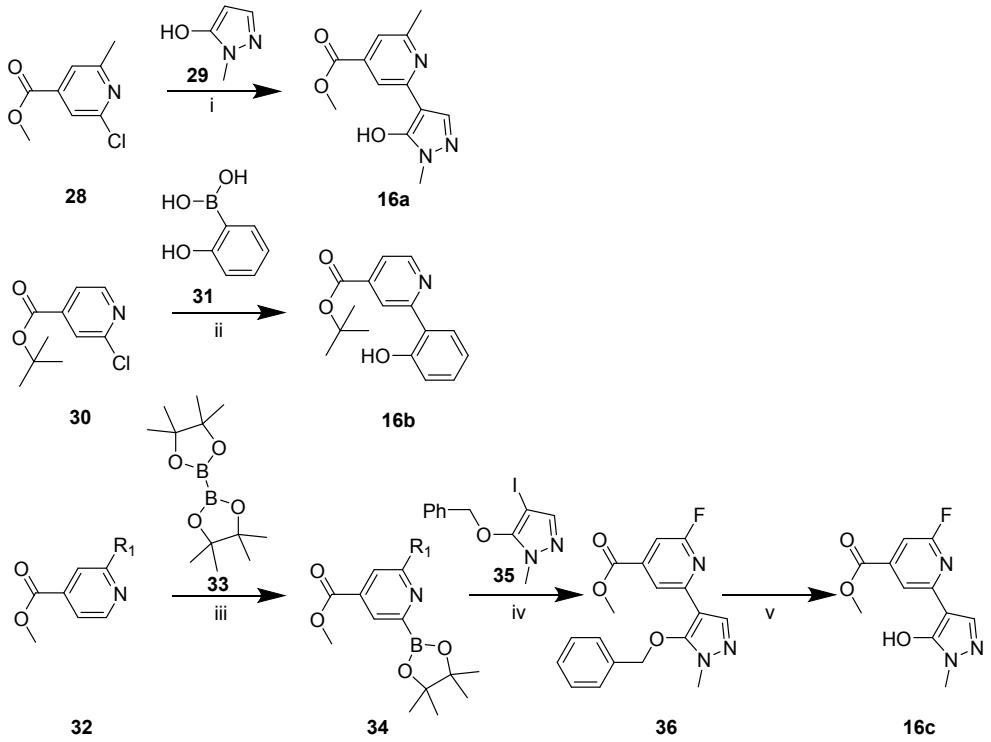

Scheme 5. Synthesis of compounds **16a-c**: Reagents and conditions: (i) $PdCl_2DPPF$, Anisole, Na_2CO_3, 130 °C, 16 h; (ii) $PdCl_2DPPF$, dioxane, K_2CO_3, 90 °C, 16 h; (iii) (1,5-cyclooctadiene)(methoxy)iridium(I) dimer, 4,4'-di-tert-butyl-2,2'-bipyridyl, 20 °C, 90 h; (iv) $PdCl_2DPPF$, dioxane, K_2CO_3, 90 °C, 1 h; (v) Pd/C, 5 bar H_2, MeOH, 20 °C, 16 h.

Key intermediate **25** was synthesized from 2-chloro-isonicotinic acid methyl ester **38** applying a CH activation reaction followed by a Suzuki coupling and ester cleavage. SEM

protection of pyrazole **29** was followed by an electrophilic aromatic substitution reaction leading to iodo-pyrazole **44** (see **Scheme 6**).

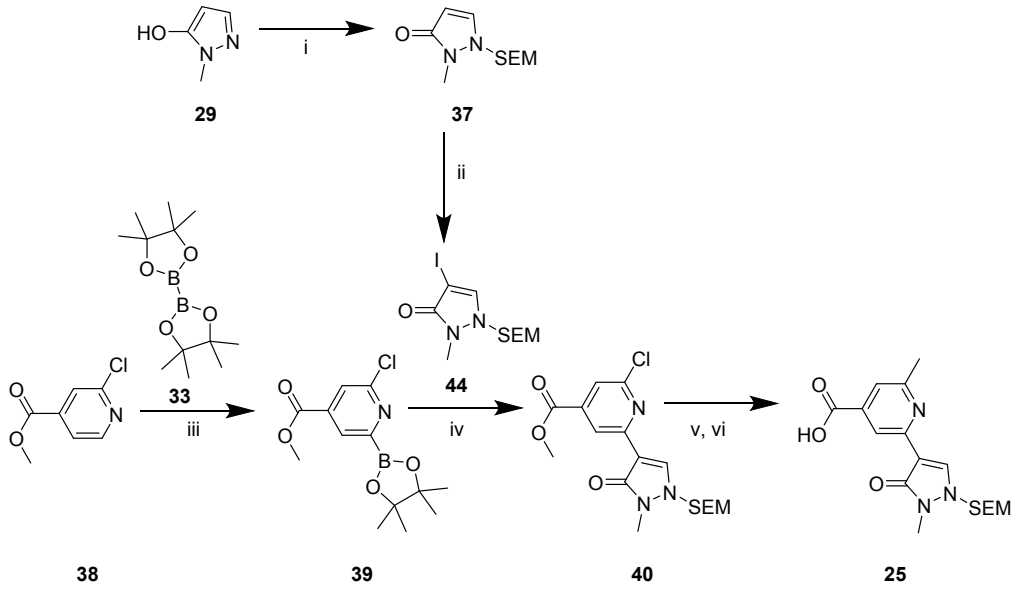

Scheme 6. Synthesis of compound **25:** Reagents and conditions: (i) SEM-Cl, K_2CO_3,ACN, 20 °C, 14 h; (ii) NIS, ACN, 0-20 °C, 2 h; (iii) (1,5-cyclooctadiene)(methoxy)iridium(I) dimer, 4,4'-di-tert-butyl-2,2'-bipyridyl, 20 °C, 66 h; (iv) Tris(dibenzylideneacetone)dipalladium, di(1 adamantyl)-n-butylphosphine, Cs_2CO_3, toluene, water, 50 °C, 2 h; (v) trimethylboroxine, tris(dibenzylideneacetone)dipalladium, di(1-adamantyl)-n-butylphosphine, Cs_2CO_3, dioxane, 80 °C, 18 h; (vi) NaOH, THF, 20 °C, 1 h.

Nucleophilic aromatic substitution reaction of amine **43** with electrophile **41** followed by an esterification with methanesulfonyl chloride led to nitroaniline **15** (see **Scheme 7**).

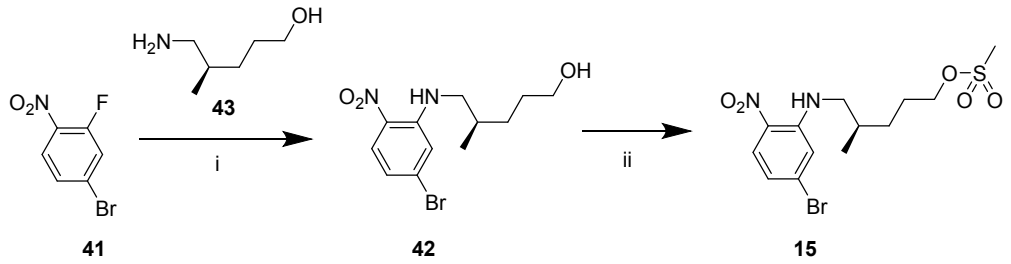

Scheme 7. Synthesis of compound **15**: Reagents and conditions: (i) K_2CO_3, DMF, 20 °C, 24 h; (ii) MsCl, NEt_3, CH_2Cl_2, 0 °C, 1 h.

CONCLUSION

The highly selective aminobenzimidazole **1** with 250 nM inhibition constant for $EGFR^{del19\ T790M\ C797S}$ was identified by screening our corporate selective kinase inhibitor library. Structure-based design and macrocyclization lead to the discovery of **BI-4020**, a highly active, non-covalent EGFR inhibitor. The strategy to increase the potency of a given ligand by restricting its conformational space to the "active" conformation by means of macrocyclization was shown to be a key contributor to success. **BI-4020** displays a single digit-nanomolar antiproliferative activity against EGFR mutant dependent cells, including cells which are dependent on EGFR bearing the two most clinically prevalent resistance mutations T790M and C797S. At the same time **BI-4020** shows a sufficient $EGFR^{wt}$ sparing window and high kinome selectivity that is comparable to the one observed with osimertinib. Furthermore **BI-4020** induces tumor regressions in the osimertinib resistant PC-9 ($EGFR^{del19\ T790M\ C797S}$) triple mutant mouse xenograft model.

Altogether, for the first time a highly active, $EGFR^{wt}$ sparing next generation EGFR TKI with an excellent *in-vitro* and *in-vivo* activity was presented. Representatives from this

promising compound class will be further profiled in *in vivo* experiments in order to be developed towards a clinical candidate, which will be active in a clinical setting where osimertinib resistance has occurred and no targeted treatment option with a TKI is available at the moment.

EXPERIMENTAL SECTION

General Remarks. Chemicals and reagents were obtained from commercial suppliers and were used without further purification. All moisture sensitive reactions were carried out under a nitrogen atmosphere in commercially available anhydrous solvents. Starting materials and intermediates are commercially available unless specified otherwise.

NMR experiments were acquired as described in the Supplementary Information.

High resolution mass spectrometry data were obtained on a LTQ Orbitrap XL (Thermo Scientific) coupled with a Triversa Nanomate Nanospray ion source (ADVION Bioscience Inc.).

Analytical HPLC-MS analyses were conducted using an Agilent 1100 series LC/MSD system. The analytic methods A1 and A2 are defined in the **Supplementary Table 1**. Compound purities were calculated as the percentage peak area of the analyzed compound by UV detection at 254 nm. If purity data is not explicitly mentioned the compound displays a purity > 95%. Flash column chromatography was carried out using

hand packed silica gel 60 (230-400 mesh) or pre-packed silica gel columns from Biotage and product was eluted under medium pressure liquid chromatography. Preparative high performance chromatography was carried out on a Gilson system (pump system: 333 & 334 prep-scale HPLC pump; fraction collector: 215 liquid handler; detector: Gilson UV/VIS 155) using pre-packed reversed phase silica gel columns from waters. The methods for preparative high performance chromatography P1-P3 are defined in the **Supplementary Table 1**.

The *in-vitro* biological data shown in this publication are the geometric mean of at least three independent measurements.

All compounds for which biology data were shown were screen for PAINS and none of them was classified as pan assay interference compound.[59,60]

3-Fluoro-N-[1-(2-hydroxy-2-methyl-propyl)-1H-benzoimidazol-2-yl]-5-pyridin-3-yl-enzamide (1).

Compound **1** was synthesized according to procedure of compound **2**.

Purity by method A1: >95%; RT = 1.27 min; MS (ESI^+) *m/z* 405 $(M+H)^+$; HRMS (m/z): [M+H]+ calculated for C23 H21 F N4 O2 , 405.17213; found, 405.17126; ^1H NMR (500 MHz, DMSO-d_6) δ 12.85 (br s, 1H), 8.97 (d, J=2.21 Hz, 1H), 8.64 (dd, J=1.42, 4.89 Hz, 1H), 8.36 (s, 1H), 8.17 (td, J=1.73, 8.20 Hz, 1H), 7.95 (dd, J=1.10, 9.30 Hz, 1H), 7.78-7.83 (m, 1H), 7.63 (dd, J=1.73, 6.78 Hz, 1H), 7.52-7.58 (m, 2H), 7.24 (ddd, J=1.42, 5.52, 7.25 Hz, 2H), 5.05 (s, 1H), 4.25 (s, 2H), 1.25 (s, 6H); ^{13}C NMR (125 MHz, DMSO-d_6) δ 171.3, 162.6 (d, J(CF)=243,4 Hz), 152.9, 149.2, 147.7, 141.6 (d, J(CF)=6,4 Hz), 139.2 (d, J(CF)=8,2 Hz), 134.4, 134.3, 130.7, 128.8, 124.0, 122.9, 122.6, 122.6, 116.2 (d, J(CF)=22,7 Hz), 114.5 (d, J(CF)=21,8 Hz), 111.9, 111.7, 71.0, 52.8, 27.9.

N-[1-(2-hydroxy-2-methyl-propyl)-1H-benzoimidazol-2-yl]-5-pyridin-3-yl-enzamide (2).

3-(Pyridin-3-yl)benzoic acid **13b** (65 mg, 0.33 mmol) and 1-(2-amino-1H-benzo[d]imidazol-1-yl)-2-methylpropan-2-ol **14** (65 mg, 0.32 mmol) were dissolved in 2 mL DMF and HATU (137 mg, 0.36 mmol) and ethyldiisopropylamine (163 µL, 0.95 mmol)

were added. The reaction mixture was stirred for 3 h at room temperature. The volatile components have been evaporated under reduced pressure and the crude product was purified applying preparative high performance chromatography method P1, yielding 94 mg (75%, 0.24 mmol) of the title compound. Purity by method A1: >95%; RT = 1.21 min; MS (ESI^+) *m/z* 387 $(M+H)^+$; HRMS (m/z): [M+H]+ calculated for C23 H22 N4 O2 , 387.18155; found, 387.18221; ^1H NMR (500 MHz, DMSO-d_6) δ 12.87 (br s, 1H), 8.94 (d, J=1.58 Hz, 1H), 8.62 (dd, J=1.58, 4.73 Hz, 1H), 8.51 (s, 1H), 8.23-8.30 (m, 1H), 8.12-8.16 (m, 1H), 7.85-7.92 (m, 1H), 7.61-7.66 (m, 2H), 7.53-7.59 (m, 1H), 7.55 (dd, J=1.58, 6.31 Hz, 1H), 7.23 (s, 2H), 5.11 (br s, 1H), 4.25 (s, 2H), 1.25 (s, 6H); ^{13}C NMR (125 MHz, DMSO-d_6) δ 172.6, 152.9, 148.6, 147.5, 139.0, 136.8, 135.6, 134.3, 130.7, 129.6, 129.0, 129.0, 128.3, 126.9, 124.1, 122.5, 111.9, 111.5, 71.0, 52.9, 27.8. Compound **1** and **3-5** were synthesized accordingly.

[2,3']Bipyridinyl-4-carboxylic acid [1-(2-hydroxy-2-methyl-propyl)-1H-benzoimidazol-2-yl]-amide (3).

Compound **3** was synthesized according to procedure of compound **2**.

Purity by method A1: >95%; RT = 1.10 min; MS (ESI^+) *m/z* 388 $(M+H)^+$; HRMS (m/z): [M+H]+ calculated for C22 H21 N5 O2 , 388.17680; found, 388.1771; ^1H NMR (500 MHz, DMSO-d_6) δ 12.94 (br s, 1H), 9.28 (d, J=1.89 Hz, 1H), 8.87 (d, J=5.04 Hz, 1H), 8.68 (dd, J=1.26, 4.73 Hz, 1H), 8.59 (s, 1H), 8.45-8.49 (m, 1H), 8.09 (dd, J=1.10, 4.89 Hz, 1H), 7.64-7.68 (m, 1H), 7.55-7.61 (m, 2H), 7.22-7.30 (m, 2H), 4.97-5.04 (m, 1H), 4.22-4.32 (m, 2H), 1.26 (s, 6H); ^{13}C NMR (125 MHz, DMSO-d_6) δ 171.1, 154.4, 152.8, 150.5, 150.0, 147.7, 146.7, 134.1, 134.0, 130.7, 128.8, 123.9, 122.7, 122.7, 121.9, 119.0, 112.0, 111.9, 71.0, 52.9, 27.9.

4'-Methoxy-[2,3']bipyridinyl-4-carboxylic acid [1-(2-hydroxy-2-methyl-propyl)-1H-benzoimidazol-2-yl]-amide (3a).

Compound **3a** was synthesized according to procedure of compound **2**.

Purity by method A1: >95%; RT = 1.08 min; MS (ESI^+) *m/z* 418 $(M+H)^+$; HRMS (m/z): [M+H]+ calculated for C23 H23 N5 O3 , 418.18737; found, 418.18740; ^1H NMR (500 MHz,

DMSO-d_6) δ 12.68-13.22 (m, 1H), 8.80 (br d, J=4.73 Hz, 1H), 8.61 (s, 1H), 8.52 (br s, 1H), 8.05 (dd, J=1.26, 5.04 Hz, 1H), 7.83 (d, J=8.20 Hz, 1H), 7.63 (d, J=8.20 Hz, 1H), 7.24-7.29 (m, 1H), 7.22 (d, J=5.67 Hz, 1H), 7.15 (t, J=7.57 Hz, 1H), 7.03 (t, J=7.57 Hz, 1H), 5.01 (s, 1H), 4.31-4.41 (m, 2H), 3.79 (s, 3H), 1.26 (s, 6H); ^{13}C NMR (125 MHz, DMSO-d_6) δ 168.8, 162.6, 156.5, 153.0, 151.4, 150.9, 150.0, 146.0, 138.0, 132.9, 124.0, 123.8, 121.6, 121.5, 121.2, 116.4, 111.3, 107.6, 71.1, 55.8, 52.9, 27.9.

N-[1-(2-Hydroxy-2-methyl-propyl)-1H-benzoimidazol-2-yl]-2-(1-methyl-1H-pyrazol-4-yl)-isonicotinamide (4).

Compound **4** was synthesized according to procedure of compound **2**.

Purity by method A1: >95%; RT = 1.06 min; MS (ESI$^+$) *m/z* 391 $(M+H)^+$; HRMS (m/z): [M+H]+ calculated for C21 H22 N6 O2 , 391.18770; found, 391.18765; ^{1}H NMR (500 MHz, DMSO-d_6) δ 12.88 (br s, 1H), 8.64 (dd, J=0.63, 5.04 Hz, 1H), 8.33 (s, 1H), 8.21 (s, 1H), 8.01 (s, 1H), 7.84 (dd, J=1.26, 4.73 Hz, 1H), 7.63-7.68 (m, 1H), 7.57 (dd, J=1.42, 7.41 Hz, 1H), 7.21-7.29 (m, 2H), 5.00 (s, 1H), 4.26 (s, 2H), 3.92 (s, 3H), 1.26 (s, 6H); ^{13}C NMR

(125 MHz, DMSO-d_6) δ 171.5, 152.8, 152.1, 149.9, 146.1, 136.9, 130.7, 129.6, 128.8, 122.8, 122.7, 122.6, 119.7, 117.7, 112.0, 111.9, 71.0, 52.8, 38.8, 27.8.

N-[1-(2-Hydroxy-2-methyl-propyl)-1H-benzoimidazol-2-yl]-2-phenyl-isonicotinamide (5).

Compound **5** was synthesized according to procedure of compound **2**.

Purity by method A1: >95%; RT = 1.31 min; MS (ESI^+) *m/z* 387 $(M+H)^+$; HRMS (m/z): [M+H]+ calculated for C23 H22 N4 O2 , 387.18155; found, 387.18197; ^1H NMR (500 MHz, DMSO-d_6) δ 12.93 (br s, 1H), 8.82 (d, J=5.04 Hz, 1H), 8.55 (s, 1H), 8.11 (d, J=7.57 Hz, 2H), 8.03 (d, J=5.04 Hz, 1H), 7.66 (br d, J=7.25 Hz, 1H), 7.52-7.59 (m, 3H), 7.45-7.51 (m, 1H), 7.21-7.29 (m, 2H), 5.02 (s, 1H), 4.27 (s, 2H), 1.27 (s, 6H); ^{13}C NMR (125 MHz, DMSO-d_6) δ 171.3, 156.6, 152.8, 150.2, 146.5, 138.7, 130.7, 129.2, 128.9, 128.8, 126.5, 122.7, 122.7, 121.2, 118.6, 112.0, 111.9, 71.0, 52.9, 27.9.

5^{1}H-11-oxa-4-aza-5(2,1)-benzo[d]imidazola-2(2,4)-pyridina-1(1,2)-benzenacycloundecaphan-3-one (6).

2-{2-[5-(2-Imino-2,3-dihydro-benzimidazol-1-yl)-pentyloxy]-phenyl}-isonicotinic acid tert-butyl ester **22b** (186 mg, 0.39 mmol) was dissolved in dichloromethane and trifluoroacetic acid (0.45 mL, 5.60 mmol) was added at room temperature. The reaction mixture was stirred for 20 hours at room temperature. After complete conversion to product the mixture was concentrated under reduced pressure. The residue was resolved in dichloromethane neutralized with 5 mL Et_3N and the mixture was concentrated under reduced pressure again. The crude product was used in next step without further purification and yield was estimated as quantitative.

2-{2-[5-(2-Imino-2,3-dihydro-benzoimidazol-1-yl)-pentyloxy]-phenyl}-isonicotonic acid as a crude product (160 mg, 0.38 mmol) was dissolved in dichloromethane and 0.17 mL Et_3N (1.15 mmol) was added at room temperature. The solution was stirred for 30 minutes at room temperature and HATU (164 mg, 0.42 mmol) was added. The reaction mixture was stirred for 16 hours at room temperature. After complete conversion to the reaction mixture was added water and it was extracted with dichloromethane. Collected organic

layers were dried over $MgSO_4$ and concentrated under reduced pressure. The crude product was purified applying preparative high performance chromatography method P3 yielding 23 mg (15%, 0.058 mmol) of the title compound.

Purity by method A1: >95%; RT = 1.48 min; MS (ESI^+) *m/z* 399 $(M+H)^+$; HRMS (m/z): [M+H]+ calculated for C24 H22 N4 O2 , 399.18155; found, 399.18060; ^1H NMR (500 MHz, DMSO-d_6) δ 12.75 (s, 1H), 9.25 (s, 1H), 8.80 (dd, J=0.63, 5.04 Hz, 1H), 8.24 (dd, J=1.73, 7.72 Hz, 1H), 7.80 (dd, J=1.42, 4.89 Hz, 1H), 7.51-7.58 (m, 2H), 7.42 (ddd, J=1.89, 7.01, 8.43 Hz, 1H), 7.28 (dtd, J=0.95, 7.65, 19.39 Hz, 2H), 7.19 (d, J=7.88 Hz, 1H), 7.09 (t, J=7.30 Hz, 1H), 4.23 (td, J=5.00, 17.10 Hz, 4H), 1.86-2.11 (m, 6H); ^{13}C NMR (125 MHz, DMSO-d_6) δ 172.4, 157.0, 154.4, 152.2, 149.6, 145.8, 130.5, 130.5, 129.3, 128.9, 126.4, 124.2, 122.9, 122.8, 120.5, 120.1, 112.6, 112.1, 109.5, 67.9, 41.2, 28.7, 28.7, 24.9.

(E)-2^6-fluoro-1^1-methyl-5^2,5^3-dihydro-1^{1}H,5^{1}H-11-oxa-4-aza-5(2,1)-benzo[d]imidazola-2(2,4)-pyridina-1(4,5)-pyrazolacycloundecaphan-3-one (7).

2-(5-{[5-(2-amino-1H-1,3-benzodiazol-1-yl]pentyloxy}-1-methyl-1H-pyrazol-4-yl)-6-fluoropyridine-4-carboxylic acid **22c** (30 mg, 0.068 mmol) and HATU (29 mg, 0.075 mmol) were suspended in 2 mL dichloromethane and 40 μl iPr2EtN (0.21 mmol) was added at room temperature. The reaction mixture was stirred for 16 hours at room temperature. After complete conversion time volatile components have been evaporated under reduced pressure.

The crude product was product was purified applying preparative high performance chromatography method P3 yielding 20 mg (70%) of the title compound.

Purity by method A1: >95%; RT = 1.34 min; MS (ESI^+) *m/z* 421 $(M+H)^+$; HRMS (m/z): [M+H]+ calculated for C22 H21 F N6 O2 , 421.17828; found, 421.17800; ^1H NMR (500 MHz, DMSO-d_6) δ 12.78 (s, 1H), 8.49 (s, 1H), 7.88 (s, 1H), 7.62 (d, J=7.88 Hz, 1H), 7.55 (d, J=7.57 Hz, 1H), 7.20-7.34 (m, 3H), 4.11-4.30 (m, 4H), 3.74 (s, 3H), 2.05 (br d, J=6.62 Hz, 4H), 1.73-1.88 (m, 2H); ^{13}C NMR (125 MHz, DMSO-d_6) δ 170.2 (d, J(CF)=3.6 Hz), 163.9 (d, J(CF)=234.3 Hz), 152.9 (d, J(CF)=7.3 Hz), 152.0, 151.7, 150.1 (d, J(CF)=14.5 Hz), 137.5, 129.8, 129.3, 123.5, 123.3, 116.7 (d, J(CF)=2.7 Hz), 112.8, 110.1, 107.0, 104.4 (d, J(CF)=39.1 Hz), 72.3, 42.9, 34.7, 28.0, 25.4, 21.9.

(E)-1^{1},2^{6}-dimethyl-5^{2},5^{3}-dihydro-1^{1}H,5^{1}H-11-oxa-4-aza-5(2,1)-benzo[d]imidazola-2(2,4)-pyridina-1(4,5)-pyrazolacycloundecaphan-3-one (8).

(E)-2-(5-hydroxy-1-methyl-1H-pyrazol-4-yl)-N-(1-(5-hydroxypentyl)-1,3-dihydro-2H-benzo[d]imidazol-2-ylidene)-6-methylisonicotinamide **26** (50 mg, 0.12 mmol) was dissolved in 5 mL anhydrous tetrahydrofurane. Diisopropyl azodicarboxylate (100 µL, 0.48 mmol) was added and the reaction vessel was purged with argon. Triphenylphosphine (130 mg, 0.47 mmol) was added and the reaction mixture was stirred at room temperature. After completion of the reaction water was added and the reaction mixture was extracted with dichloromethane. The combined organic layers were dried over magnesium sulfate and concentrated. The residue was purified applying preparative high performance chromatography (method P1), yielding 31 mg (65%, 0.07 mmol) of the title compound.

Purity by method A1: >95%; RT = 1.30 min; MS (ESI^{+}) *m/z* 417 $(M+H)^{+}$; HRMS (m/z): [M+H]+ calculated for C23 H24 N6 O2 , 417.20335; found, 417.20338; ^{1}H NMR (500 MHz,

DMSO-d_6) δ 12.67 (br s, 1H), 8.41 (s, 1H), 7.92 (s, 1H), 7.59 (d, J=7.57 Hz, 1H), 7.57 (d, J=0.63 Hz, 1H), 7.54 (d, J=7.50 Hz, 1H), 7.28 (ddd, J=1.50, 7.00, 8.10 Hz, 1H), 7.23 (ddd, J=1.00, 7.00, 8.10 Hz, 1H), 4.17-4.24 (m, 4H), 3.73 (s, 3H), 2.56 (s, 3H), 1.99-2.12 (m, 4H), 1.75-1.84 (m, 2H); ^{13}C NMR (125 MHz, DMSO-d_6) δ 171.6, 158.0, 151.7, 150.7, 150.4, 146.3, 136.9, 129.4, 128.9, 122.8, 122.6, 118.2, 115.7, 112.2, 109.4, 107.8, 71.6, 42.3, 34.1, 27.5, 24.8, 24.5, 21.3.

(R,E)-1^1,2^6,7-trimethyl-5^2,5^3-dihydro-1^{1}H,5^{1}H-11-oxa-4-aza-5(2,1)-benzo[d]imidazola-2(2,4)-pyridina-1(4,5)-pyrazolacycloundecaphan-3-one (9).

(R,E)-5^6-bromo-1^1,2^6,7-trimethyl-5^2,5^3-dihydro-11H,51H-11-oxa-4-aza-5(2,1)-benzo[d]imidazola-2(2,4)-pyridina-1(4,5)-pyrazolacycloundecaphan-3-one **9Br** (100 mg, 0.20 mmol) was dissolved in 3 ml DMF and then triethysilane (0.32 ml, 1.91 mmol), sodium carbonate (72 mg, 0.68 mmol) and [1,1'-bis(diphenylphosphino)ferrocene]dichloropalladium (II) (4 mg, 0,005 mmol) were added

at 25°C. The reaction mixture is stirred at 90 °C for 16 h and afterwards it was filtered over celite and the solvents were removed under reduced pressure. The residue was purified applying preparative high performance chromatography (method P1), yielding 21 mg (25%, 0.05 mmol) of the title compound.

Purity by method A1: >95%; RT = 1.36 min; MS (ESI^+) *m/z* 431 $(M+H)^+$; ^1H NMR (500 MHz, DMSO-d_6) δ 12.74 (br s, 1H), 8.43 (s, 1H), 7.92 (s, 1H), 7.60 (d, J=7.88 Hz, 1H), 7.57 (s, 1H), 7.55 (d, J=7.57 Hz, 1H), 7.28 (t, J=7.70 Hz, 1H), 7.23 (t, J=7.70 Hz, 1H), 4.35 (td, J=4.49, 9.30 Hz, 1H), 4.20 (dd, J=2.84, 13.56 Hz, 1H), 3.97-4.04 (m, 1H), 3.93 (dd, J=10.40, 13.56 Hz, 1H), 3.73 (s, 3H), 2.80 (br d, J=3.47 Hz, 1H), 2.56 (s, 3H), 2.15-2.27 (m, 1H), 1.85-2.04 (m, 2H), 1.39-1.51 (m, 1H), 0.81 (d, J=6.62 Hz, 3H); ^{13}C NMR (125 MHz, DMSO-d_6) δ 171.3, 158.0, 151.6, 150.8, 150.4, 146.2, 136.9, 130.4, 128.8, 122.9, 122.5, 118.2, 115.7, 112.2, 109.7, 107.8, 71.3, 49.4, 34.1, 28.8, 28.7, 25.5, 24.5, 16.8.

(R,E)-5^6-bromo-1^1,2^6,7-trimethyl-5^2,5^3-dihydro-11H,51H-11-oxa-4-aza-5(2,1)-benzo[d]imidazola-2(2,4)-pyridina-1(4,5)-pyrazolacycloundecaphan-3-one (9Br).

(R)-2-(5-((5-(2-Amino-6-bromo-1H-benzo[d]imidazol-1-yl)-4-methylpentyl)oxy)-1-methyl-1H-pyrazol-4-yl)-6-methylisonicotinic acid **22a'** (9.70 g, 18.4 mmol) was dissolved in CH_2Cl_2 (200 mL) and Et_3N (10.3 mL, 73.6 mmol) was added. To the resultant solution was added TBTU (7.09 g, 22.1 mmol) and the reaction mixture was stirred at room temperature for 15 min. The reaction mixture was washed with water (3 x 100 mL) and the organic phase was dried over Na_2SO_4, filtered, and concentrated under reduced pressure. The crude product was purified by chromatography on SiO_2 using CH_2Cl_2/MeOH (100:0 to 95:5) as eluent. The resultant material was further purified by recrystallization from hot toluene to give the title compound (5.24 g, 10.3 mmol, 56%) as a white solid. Purity by method A1: >95%; RT = 1.46 min; MS (ESI^+) *m/z* 509/511 $(M+H)^+$; HRMS (m/z): [M+H]+ calculated for C24 H25 Br N6 O2,509.12948; found, 509.12799; ^1H NMR (400 MHz, DMSO-d_6) δ 12.84 (br s, 1H), 8.41 (s, 1H), 7.92 (s, 2H), 7.56 (s, 1H), 7.47 (d, J=8.40 Hz, 1H), 7.39 (dd, J=1.80, 8.40 Hz, 1H), 4.28-4.41 (m, 1H), 4.11-4.20 (m,

1H), 3.93-4.05 (m, 2H), 3.73 (s, 3H), 2.72-2.87 (m, 1H), 2.56 (s, 3H), 2.14-2.28 (m, 1H), 1.84-2.05 (m, 2H), 1.37-1.51 (m, 1H), 0.81 (d, J=6.59 Hz, 3H); ^{13}C NMR (100 MHz, DMSO-d_6) δ 172.1, 158.5, 152.4, 151.2, 150.9, 146.4, 137.4, 132.4, 128.6, 125.7, 118.6, 116.2, 115.5, 114.3, 113.0, 108.2, 71.7, 50.0, 34.6, 29.1, 29.0, 26.0, 24.9, 17.1.

(R,E)-11,26,7-trimethyl-56-((4-methylpiperazin-1-yl)methyl)-52,53-dihydro-11H,51H-11-oxa-4-aza-5(2,1)-benzo[d]imidazola-2(2,4)-pyridina-1(4,5)-pyrazolacycloundecaphan-3-one (BI-4020).

(*R*,*E*)-11,26,7-trimethyl-3-oxo-52,53-dihydro-11H,51H-11-oxa-4-aza-5(2,1)-benzo[d]imidazola-2(2,4)-pyridina-1(4,5)-pyrazolacycloundecaphane-56-carbaldehyde **27** (2.00 g, 3.82 mmol, 87% purity) and 1-methylpiperazine (2.83 g, 28.25 mmol) were dissolved in 40 ml DCM and AcOH (1.99 g, 19.86 mmol) and sodium triacetoxyborohydride (2.26 g, 10.7 mmol) were added sequentially. The reaction mixture was stirred for 6 h at room temperature. The reaction was quenched with sat. $NaHCO_3$ (15 ml) and the volatile components were evaporated under reduced pressure. The crude

residue was partitioned between 2-methyltetrahydrofuran (25 ml) and sat. NH_4Cl (20 ml), and the resulting organic layer was washed with 5% brine (25 ml). The final organic layer was dried over magnesium sulfate and concentrated under reduced pressure to dryness and the crude product was purified by Combiflash using 10% MeOH in DCM (R_f 0.18 in 10% MeOH in DCM) yielding 1.5 g of off-white foam (72.4%, 2.76 mmol) of the desired product **BI-4020**. Purity by method A1: >95%; RT = 1.26 min; MS (ESI^+) *m/z* 543 $(M+H)^+$; HRMS (m/z): [M+H]+ calculated for C30 H38 N8 O2 , 543.31905; found, 543.31976; ^1H NMR (500 MHz, DMSO-d_6) δ 12.67 (br s, 1H), 8.42 (s, 1H), 7.92 (s, 1H), 7.56 (s, 1H), 7.49 (s, 1H), 7.47 (d, J=8.20 Hz, 1H), 7.43-7.48 (m, 1H), 7.16 (dd, J=0.95, 8.20 Hz, 1H), 4.35 (td, J=4.57, 9.14 Hz, 1H), 4.19 (dd, J=2.99, 13.71 Hz, 1H), 3.96-4.03 (m, 1H), 3.92 (dd, J=10.09, 13.56 Hz, 1H), 3.71-3.75 (m, 1H), 3.73 (s, 2H), 3.55 (d, J=3.15 Hz, 2H), 2.72-2.85 (m, 1H), 2.55 (s, 3H), 2.17-2.47 (m, 8H), 2.14 (s, 3H), 1.86-2.03 (m, 2H), 1.40-1.52 (m, 1H), 0.80 (d, J=6.62 Hz, 3H); ^{13}C NMR (125 MHz, DMSO-d_6) δ 171.3, 157.9, 151.7, 150.8, 150.4, 146.2, 136.9, 133.4, 130.4, 127.8, 123.5, 118.2, 115.7, 111.8, 109.8, 107.8, 71.3, 62.2, 54.7, 52.5, 49.3, 45.7, 34.1, 28.7, 28.7, 25.5, 24.5, 16.8.

4-carboxy-4'-methoxy-[2,3'-bipyridin]-1'-ium chloride (13d).

Tert-butyl-2-bromoisonicotinate (6.50 g; 25.18 mmol), monolithium 4-methoxypyridine-3-boronate (8.17 g; 50.37 mmol), tri-tert-butylphosphonium tetrafluoroborate (731 mg; 2.52 mmol) and palladium (II) acetate (565 mg; 2.52 mmol) were dissolved in 195 mL 1,2-dimethoxyethane and 65 mL water. The mixture was flushed with argon and stirred at room temperature for 5 min. Then cesium carbonate (13.95 g; 42.81 mmol) was added and stirring was continued at 80°C for 16 hours. The reaction mixture was poured on water and extracted with DCM once. The organic layer was dried over MgSO4 and concentrated under reduced pressure. The residue was purified applying preparative high performance chromatography (method P3). The resulting tert-butyl 2-(4-methoxypyridin-3-yl)pyridine-4-carboxylate (4.86 g; 16.12 mmol) was dissolved in 276 mL acetonitrile and 11 mL of concentrated hydrochloric acid (131.08 mmol) were added. The mixture was stirred at 55°C for 16 hours. The precipitate was filtered off, washed with cold acetonitrile and dried in vacuum to give 4.18 g (62%, 15.69 mmol) of the title compound.

Purity by method A2: 96%; RT = 0.21 min; MS (ESI^+) *m/z* 231 $(M+H)^+$;

(R)-5-((5-bromo-2-nitrophenyl)amino)-4-methylpentyl methanesulfonate (15)

(R)-5-((5-bromo-2-nitrophenyl)amino)-4-methylpentan-1-ol **42** (20.0 g, 63.2 mmol) and Et_3N (13.2 mL, 94.8 mmol) were mixed with CH_2Cl_2 (85 mL) and the resultant solution was cooled to 0 °C. MsCl (5.87 mL, 75.8 mmol) was added dropwise at 0 °C, and upon completion of the addition the cooling bath was removed and the reaction mixture allowed to stir at room temperature for 1 h. The mixture was then washed sequentially with saturated aqueous $NaHCO_3$ solution and water, and the organic phase was dried over Na_2SO_4, filtered and concentrated under reduced pressure to yield the title compound (24.7 g, 62.5 mmol, 99%) as an orange oil. HRMS (m/z): [M+H]+ calculated for C13 H20 Br N2 O5 S, 395.02708; found, 395.02683; ^{1}H NMR (400 MHz, $CDCl_3$) δ 8.09 (br, 1H), 7.97 (d, J=9.07 Hz, 1H), 6.96 (d, J=1.98 Hz, 1H), 6.71 (dd, J=1.98, 9.08 Hz, 1H), 4.22 (t, J=6.31 Hz, 2H), 3.21-3.15 (m, 1H), 3.11-3.05 (m, 1H), 2.99 (s, 3H), 1.93-1.70 (m, 3H), 1.64-1.55 (m, 1H), 1.41-1.30 (m, 1H), 1.04 (d, J=6.69 Hz, 3H); ^{13}C NMR (100 MHz, $CDCl_3$) δ 145.9, 131.8, 130.8, 128.2, 118.6, 116.4, 69.8, 49.1, 37.4, 32.3, 30.3, 26.6, 17.8.

Methyl 2-(5-hydroxy-1-methyl-1H-pyrazol-4-yl)-6-methylisonicotinate hydrochloride (16a)

Methyl 2-chloro-6-methylisonicotinate **28** (50.0 g, 269.4 mmol), 1-methyl-1H-pyrazol-5-ol **29** (52.9 g, 538.8 mmol), $PdCl_2(dppf)\bullet CH_2Cl_2$ (6.60 g, 8.08 mmol), powdered Na_2CO_3 (62.8 g, 592.7 mmol) and anisole (1000 mL) was heated at 130 °C under nitrogen for 16 h. The reaction mixture was then cooled to room temperature and was filtered through a 2 cm pad of Celite. The Celite pad was washed with toluene (200 mL). The dark filtrate was treated with MeOH (150 mL) followed by dropwise addition of 4M HCl in dioxane (100 mL, 400 mmol). The resultant slurry was stirred at room temperature for 1 h and then was filtered. The filter cake was washed with toluene and heptane, and was then dried under vacuum at 50 °C to yield the title compound (47.5 g, 98.4 wt.%, 164.7 mmol, 61%) as a yellow solid. HRMS (m/z): [M+H - HCl]+ calculated for C12 H14 N3 O3, 248.10297; found, 248.10291; ^{1}H NMR (400 MHz, D_2O) δ 8.17 (s, 1H), 8.03 (m, 1H), 7.65 (m, 1H), 3.91 (s, 3H), 3.42 (s, 3H), 2.63 (s, 3H); ^{13}C NMR (100 MHz, D_2O) δ 164.3, 160.3, 151.9, 147.9, 143.8, 132.5, 120.1, 117.9, 95.5, 53.9, 30.2, 19.3.

Methyl (R)-2-(5-((5-((5-bromo-2-nitrophenyl)amino)-4-methylpentyl)oxy)-1-methyl-1H-pyrazol-4-yl)-6-methylisonicotinate (17)

(R)-5-((5-bromo-2-nitrophenyl)amino)-4-methylpentyl methanesulfonate **15** (13.8 g, 95% purity, 33.1 mmol) and methyl 2-(5-hydroxy-1-methyl-1H-pyrazol-4-yl)-6-methylisonicotinate hydrochloride **16a** (9.63 g, 33.9 mmol) were dissolved in DMF (50 mL). Then K_2CO_3 (11.4 g, 82.8 mmol) was added and the mixture was stirred at 60 °C for 18 h. The reaction mixture was then cooled to room temperature, diluted with methyl tert-butyl ether, and washed twice with water. The organic phase was then dried over Na_2SO_4, filtered and concentrated under reduced pressure to yield the title compound (15.4 g, 28.2 mmol, 85%) as an orange oil. HRMS (m/z): [M+H]+ calculated for C24 H29 Br N5 O5, 546.13466; found, 546.13479; ^{1}H NMR (400 MHz, $CDCl_3$) δ 8.16 (br m, 1H), 8.01 (d, J = 9.12 Hz, 1H), 7.88 (s, 1H), 7.87-7.86 (m, 1H), 7.48-7.47 (m, 1H), 7.00 (d, J = 1.94 Hz, 1H), 6.73 (dd, J = 1.98, 9.09 Hz, 1H), 4.16 (t, J = 6.39 Hz, 2H), 3.94 (s, 3H), 3.75 (s, 3H), 3.28-3.22 (m, 1H), 3.16-3.10 (m, 1H), 2.61 (s, 3H), 2.02-1.81 (m, 3H), 1.77-1.69 (m, 1H),

1.53-1.43 (m, 1H), 1.10 (d, J = 6.67 Hz, 3H); ^{13}C NMR (100 MHz, $CDCl_3$) δ 166.1, 159.1, 152.2, 151.4, 145.9, 138.0, 137.9, 131.7, 130.8, 128.2, 118.9, 118.6, 116.3, 107.3, 74.8, 52.6, 49.2, 34.3, 32.6, 30.8, 27.3, 24.7, 17.8.

Methyl (R)-2-(5-((5-((2-amino-5-bromophenyl)amino)-4-methylpentyl)oxy)-1-methyl-1H-pyrazol-4-yl)-6-methylisonicotinate (18)

Methyl (R)-2-(5-((5-((5-bromo-2-nitrophenyl)amino)-4-methylpentyl)oxy)-1-methyl-1H-pyrazol-4-yl)-6-methylisonicotinate **17** (2.75 g, 5.03 mmol) and 50% wet catalyst 1%Pt/2%V/C (2.4 g, 0.015 mmol Pt) were added to a 100 mL hydrogenation autoclave, followed by addition of MeOH (40 mL). The reaction mixture was purged with nitrogen 3 times and then with hydrogen once, followed by hydrogenation under 100 psi H_2 at 20 °C for 16 h. The reaction mixture was filtered through Celite to remove the catalyst and then the solvent was removed under reduced pressure to yield the title compound (2.54 g, 4.92 mmol, 98%) as a dark oil. HRMS (m/z): [M+H]+ calculated for C24 H31 Br N5 O3, 516.16048; found, 526.16075; ^{1}H NMR (400 MHz, $CDCl_3$) δ 7.81 (s, 2H), 7.80 (m, 1H),

7.41 (br s, 1H), 6.66 (dd, J = 2.1, 8.1 Hz, 1H), 6.49 (d, J = 2.1 Hz, 1H), 4.06 (t, J = 6.4 Hz, 1H), 3.88 (s, 3H), 3.67 (s, 3H), 3.05 (br s, 3H), 2.95 (dd, J = 6.4, 12.2 Hz, 1H), 2.85 (dd, J = 6.4, 12.0 Hz, 1H), 2.54 (s, 3H), 1.76 (m, 4H), 1.34 (m, 1H), 0.97 (d, J = 6.5 Hz, 3H); ^{13}C NMR (100 MHz, $CDCl_3$) δ 166.2, 159.2, 152.2, 151.6, 139.6, 138.1, 138.0, 132.7, 120.5, 119.0, 117.8, 116.4, 114.0, 113.3, 107.3, 75.1, 52.6, 50.2, 34.3, 32.8, 30.9, 27.4, 24.7, 18.0.

Methyl (R)-2-(5-((5-(2-amino-6-bromo-1H-benzo[d]imidazol-1-yl)-4-methylpentyl)oxy)-1-methyl-1H-pyrazol-4-yl)-6-methylisonicotinate (22a)

Methyl (R)-2-(5-((5-((2-amino-5-bromophenyl)amino)-4-methylpentyl)oxy)-1-methyl-1H-pyrazol-4-yl)-6-methylisonicotinate **18** (2.60 g, 5.03 mmol) was dissolved in CH_2Cl_2 (25 mL) and *tert*-butanol (5 mL). The resultant solution was treated with cyanogen bromide (0.64 g, 6.04 mmol) and the reaction mixture was stirred at room temperature for 18 h. The reaction mixture was treated with saturated aqueous $NaHCO_3$ solution and stirred for 10 min. The layers were separated, and the organic phase was washed again

with saturated aqueous $NaHCO_3$ solution. The organic phase was then dried over Na_2SO_4, filtered and concentrated under reduced pressure to yield the title compound (2.26 g, 4.17 mmol, 83%) as a dark foamy solid. This compound was difficult to purify by chromatography or crystallization and was taken into the next steps directly. HRMS (m/z): [M+H]+ calculated for C25 H30 Br N6 O3, 541.15573; found, 541.15537; ^{1}H NMR (400 MHz, $CDCl_3$) δ 7.89-7.87 (m, 2H), 7.47-7.46 (m, 1H), 7.27-7.19 (m, 3H), 4.11-4.06 (m, 2H), 3.94 (s, 3H), 3.86-3.81 (m, 1H), 3.75-3.69 (m, 1H), 3.68 (s, 3H), 2.60 (s, 3H), 2.19-2.11 (m, 1H), 2.00-1.92 (m, 1H), 1.83-1.66 (m, 2H), 1.48-1.38 (m, 1H), 0.99 (d, J = 6.63 Hz, 3H); ^{13}C NMR (100 MHz, $CDCl_3$) δ 166.3, 159.3, 154.2, 152.2, 151.4, 140.4, 137.98, 137.95, 135.6, 124.6, 119.0, 117.3, 116.3, 112.4, 111.1, 107.4, 74.8, 52.7, 49.2, 34.3, 33.2, 30.7, 27.2, 24.7, 17.4.

(R)-2-(5-((5-(2-Amino-6-bromo-1H-benzo[d]imidazol-1-yl)-4-methylpentyl)oxy)-1-methyl-1H-pyrazol-4-yl)-6-methylisonicotinic acid (22a')

Methyl (R)-2-(5-((5-(2-amino-6-bromo-1H-benzo[d]imidazol-1-yl)-4-methylpentyl)oxy)-1-methyl-1H-pyrazol-4-yl)-6-methylisonicotinate **22a** (1.80 g, 3.32 mmol) was dissolved in THF (30 mL). To the reaction mixture was added a solution of NaOH pellets (0.53 g, 13.3 mmol) in water (30 mL). The reaction mixture was stirred at room temperature for 45 min, and then the THF was removed by distillation under reduced pressure. The solution was acidified with 6M aqueous HCl to pH = 5, resulting in the formation of a slurry. The solid was filtered and washed with water, and dried under vacuum to yield the title compound (1.71 g, 3.24 mmol, 98%) as a dark solid. HRMS (m/z): [M+H]+ calculated for C24 H28 Br N6 O3, 527.14008; found, 527.13971; ^{1}H NMR (400 MHz, DMSO-d_6) δ 7.89-7.84 (m, 2H), 7.70-7.53 (m, 2H), 7.46 (m, 2H), 7.12 (br s, 2H), 4.07 (br, 2H), 3.98-3.84 (m, 2H), 3.63 (s, 3H), 2.51 (s, 3H), 2.12-2.00 (m, 1H), 1.99-1.85 (m, 1H), 1.82-1.67 (m, 1H), 1.66-1.50 (m, 1H), 1.47-1.29 (m, 1H), 0.83 (d, J = 6.26 Hz, 3H); ^{13}C NMR (100 MHz, DMSO-d_6) δ 168.5, 158.7, 155.0, 151.6, 151.5, 142.1, 137.6, 137.5, 135.1, 124.4, 119.5, 116.2, 115.3, 112.0, 111.8, 107.6, 75.4, 48.0, 34.5, 32.5, 30.1, 27.1, 24.7, 16.7.

(R,E)-11,26,7-trimethyl-3-oxo-52,53-dihydro-11H,51H-11-oxa-4-aza-5(2,1)-benzo[d]imidazola-2(2,4)-pyridina-1(4,5)-pyrazolacycloundecaphane-56-carbaldehyde (27).

(R,E)-5^6-bromo-1^1,2^6,7-trimethyl-5^2,5^3-dihydro-11H,51H-11-oxa-4-aza-5(2,1)-benzo[d]imidazola-2(2,4)-pyridina-1(4,5)-pyrazolacycloundecaphan-3-one **9Br** (2.27 g, 4.46 mmol), $Pd(OAc)_2$ (50.0 mg, 0.223 mmol), di(1-adamantyl)-*n*-butylphosphine (240 mg, 0.668 mmol), dioxane (34 mL), and TMEDA (1.34 mL, 8.91 mmol) were charged to a HEL reactor under nitrogen. The reaction mixture was heated to 100 °C for 24 h under 80 psi of CO/H_2 syngas. After cooling to room temperature, the reaction was filtered through a filter paper to remove precipitates, and the filtrate was concentrated under reduced pressure. The crude residue was purified by flash chromatography on SiO_2 using an elution gradient of 0 to 4% MeOH in CH_2Cl_2. The title compound was obtained as a white solid (2.00 g, 3.80 mmol, 85%). HRMS (m/z): [M+H]+ calculated for C25 H27 N6 O3, 459.21392; found, 459.21363; ^{1}H NMR (400 MHz, $CDCl_3$) δ 12.27 (br s, 1H), 10.04 (s, 1H), 8.47 (s, 1H), 8.16 (s, 1H), 7.83 (d, J = 0.9 Hz, 1H), 7.77 (dd, J = 8.1, 1.3 Hz, 1H),

7.64 (d, J = 0.9 Hz, 1H), 7.47 (d, J = 8.1 Hz, 1H), 4.45 (m, 1H), 4.38 (m, 1H), 3.89 (m, 1H), 3.78 (two overlapping peaks, 4H), 2.86 (m, 1H), 2.63 (s, 3H), 2.28 (m, 1H), 2.1 (m, 1H), 1.98 (m, 1H), 1.55 (m, 1H), 0.93 (d, J = 6.6 Hz, 3H); ^{13}C NMR (100 MHz, $CDCl_3$) δ 191.0, 175.2, 159.0, 154.4, 151.3, 151.2, 145.3, 138.4, 133.2, 132.5, 131.5, 127.3, 118.8, 116.8, 111.5, 108.9, 71.3, 50.6, 34.3, 29.61, 29.59, 26.4, 24.9, 17.7.

(R)-5-((5-bromo-2-nitrophenyl)amino)-4-methylpentan-1-ol (42)

4-Bromo-2-fluoro-1-nitrobenzene **41** (14.0 g, 63.6 mmol), (*R*)-5-amino-4-methylpentan-1-ol hydrochloride **43** (10.5 g, 97.7 wt.%, 66.8 mmol) and K_2CO_3 (19.3 g, 140.0 mmol) were stirred in DMF (42 mL) for 24 h at room temperature. The reaction mixture was then diluted with water and extracted with methyl tert-butyl ether. The organic phase was dried over Na2SO4, filtered and concentrated under reduced pressure to yield the title compound (20.0 g, 63.2 mmol, 99%) as an orange oil. HRMS (m/z): [M+H]+ calculated for C12 H18 Br N2 O3, 317.04953; found, 317.04942; ^{1}H NMR (400 MHz, $CDCl_3$) δ 8.10 (br, 1H), 7.96 (d, J=9.14 Hz, 1H), 6.95 (d, J=1.98 Hz, 1H), 6.68 (dd, J=1.95, 9.08 Hz, 1H),

3.63 (t, J=6.39 Hz, 2H), 3.21-3.15 (m, 1H), 3.08-3.02 (m, 1H), 2.04 (s, 1H), 1.91-1.83 (m, 1H), 1.71-1.48 (m, 3H), 1.35-1.26 (m, 1H), 1.03 (d, J=6.74 Hz, 3H); ^{13}C NMR (100 MHz, $CDCl_3$) δ 146.0, 131.8, 130.7, 128.1, 118.5, 116.4, 62.8, 49.2, 32.5, 30.7, 29.9, 18.0.

Protein production, crystallization and structure determination

An EGFR kinase construct comprising amino acids 696-1022 was expressed as a GST-fusion protein in insect cells. In addition to the mutations T790M, L858R the construct also contained three mutations to improve crystallization with “EEK” (865-867) mutated to “AAA” as described by Hanan et al., 2004.[61] Protein was purified by a three-step procedure using a 20mL GSTrap-column (GE Health Care), followed by tag-cleavage with thrombin, a second passage over the GSTrap column and a final gel filtration step on a Superdex75 26/60 column (GE Health Care). Pure and monomeric protein was pooled, buffer exchanged into 25 mM TRIS/HCl, pH = 8.0, 100 mM NaCl, 2 mM DTT, 2 mM TCEP, concentrated to 11mg/mL and stored in aliquots at -80°C until crystallization.

For crystallization the protein was diluted to 8 mg/mL. Crystals were grown at 20°C from 10% PEG10000, 8% ethylene glycol, 0.10 M HEPES pH 7.5 by hanging drop method. For crystallization 1 µL of the protein solution were mixed with 0.5 µL of the reservoir solution and placed over 300 µL of the reservoir solution in 15 well plates (Qiagen). Ligand complexes were generated by soaking apo crystals with 5mM of the respective ligand for

3 hours. For cryo protection crystals were briefly immersed in reservoir solution containing 20% (v/v) L-(+)-2,3-butanediol and frozen in liquid nitrogen.

Diffraction data were measured at 100 K at the Swiss Light Source (beamline PXI/X06SA). Data were integrated with XDS and scaled with XSCALE.[62] Molecular replacement for performed with MOLREP.[63] The structures were refined with REFMAC.[64]

Protein crystallography has been done by Proteros Biostructures (Martinsried). Coordinates and structure factors have been deposited at the PDB with PDB codes 6S9B (compound **1**), 6S9C (compound **5**) and 6S9D (compound **6**).

Biochemical EGFR inhibition assays

These assays measure the inhibitory effect of compounds on the phosphorylation activity of EGFR enzyme forms on poly-GT substrate in the presence of ATP.

The following enzyme forms of EGFR have been used in these assays at the given concentrations:

- EGFR WT (Life technologies; PV4190); final assay concentration 1.5 nM

- EGFR (d746-750 T790M C797S) (SignalChem; E10-12UG); final assay concentration 15 nM

Test compounds dissolved in DMSO were dispensed onto assay plates (Proxiplate 384 PLUS, white, PerkinElmer; 6008289) using an Access Labcyte Workstation with the Labcyte Echo 55x. For the chosen highest assay concentration of 100 µM, 150 nL of compound solution was transferred from a 10 mM DMSO compound stock solution. A series of eleven fivefold dilutions per compound was transferred to the assay plate, compound dilutions were tested in duplicates. DMSO was added as backfill to a total volume of 150 nL. The assay runs on a fully automated robotic system.

5µL of EGFR enzyme form in assay buffer (50mM HEPES pH 7.3, 10mM MgCl2, 1mM EGTA, 0.01% Tween 20, 2mM DTT) are dispensed into columns 1-23, than 5µL of ATP and ULight-poly-GT substrate (PertkinElmer; TRF0100-M) mix in assay buffer is added to all wells (final assay concentration of ATP 100 µM and ULight-poly-GT substrate 200 nM).

After 90 minutes incubation at room temperature 5µL EDTA (final assay concentration 50 mM) and LANCE Eu-anti-P-Tyr (PT66) antibody (PerkinElmer, AD0069) (final assay

concentration 6 nM) mix are added to stop the reaction and start the binding of the antibody.

After additional 60 minutes incubation at room temperature the signal is measured in a PerkinElmer Envision HTS Multilabel Reader using the TR-FRET LANCE Ultra specs of PerkinElmer (used wavelengths: excitation 320 nm, emission1 665 nm, emission2 615 nm).

Each plate contains 16 wells of a negative control (diluted DMSO instead of test compound; w EGFR enzyme form; column 23) and 16 wells of a positive control (diluted DMSO instead of test compound; w/o EGFR enzyme form; column 24).

Negative and positive control values were used for normalization and IC_{50} values were calculated and analysed using a 4 parametric logistic model.

These biochemical EGFR enzyme form compound dose-response assays quantify the kinase activity via phosphorylation of a tagged poly-GT substrate. The results of the assay are provided as IC50 values. The lower the reported biochemical EGFR enzyme form IC50 values for a given compound, the more potent the compound inhibits the EGFR enzyme form kinase activity on poly-GT substrate.

Ba/F3 proliferation data

Ba/F3 cells (purchased from DSMZ, Cat.No. ACC300) were grown in RPMI-1640 medium supplemented with 10% FCS at 37 °C in 5% CO_2 atmosphere in the presence of 10 ng/mL IL-3 (purchased from R&D). To generate Ba/F3 EGFR models Ba/F3 cells were transduced with retroviruses encoding the Green Fluorescent Protein (GFP) and EGFR isoforms EGFRwt, EGFRdel19 or EGFRdel19 TM CS. Platinum-E cells (Cell Biolabs) were used for retrovirus packaging. Ba/F3 cells were transduced with a retrovirus encoding only GFP to generate EGFR-independent Ba/F3 cells. Retrovirus and 4µg/mL polybrene was added to Ba/F3 cells for spinfection. Infection efficiency was confirmed by measuring GFP-positive cells using a cell analyzer. Cells with an infection efficiency of 10% to 20% were further cultivated in the presence of Puromycin (1 µg/mL) to select for transduced cells. Following selection IL-3 was withdrawn from transgenic Ba/F3 cells expressing the oncogenic EGFR alleles EGFRdel19 and EGFRdel19 TM CS to render the growth of the cells dependent on transgenic EGFR activity. At IL-3 withdrawal EGF ligand (conc., source) was added to cells expressing EGFRwt, which are dependent on

ligand stimulation in the absence of IL-3. Empty vector-transduced cells were maintained in medium containing IL-3 to generate EGFR-independent control cells. For proliferation assays BaF/3 cells were seeded into a 96-well plates at 5x103/100 µl in growth media. Compounds were added by using a HP D3000 Digital Dispenser. All treatments were performed in technical and biological triplicates. Treated cells were incubated for 72h at 37 °C with 5% CO2. CellTiter-Glo® Luminescent Cell Viability Assay (Promega) was performed and chemoluminescence was measured by using the multilabel Plate Reader VICTOR X4. The raw data were imported into and analyzed with the Boehringer Ingelheim proprietary software MegaLab (curve fitting based on the program PRISM, GraphPad Inc.).

Ba/F3 p-EGFR Biomarker Assay

60.000 Ba/F3 EGFRdel19 TM CS expressing cells were seeded in 60 µL DMEM with 10% FBS per well into a TC 384-well plate (Greiner 781182). 60 nL compound solution was added with the Echo Access System (Labcyte). All treatments were done in

technical and biological duplicates. Treated cells were incubated for 4h at 37 °C with 5% CO2. Plates were then centrifuged for 10 min, medium removed by the EL406 Washer and replaced by 20 µL of a 1.6-fold lysis buffer of the p-EGF Receptor (p-Tyr1068) TGRERS kit (PerkinElmer). After incubation at RT with agitation on a plate shaker (700 rpm) for 20minutes, plates were centrifuged for 5 minutes and 4 µL of the lysate transferred to a Proxiplate™-384 Plus (PerkinElmer). 5 µL Acceptor Mix (Reaction buffer + Activation buffer + AlphaScreen® Acceptor beads, PerkinElmer) were added, plates shaken for 1 minute (14000 rpm) and incubated for 2h at room temperature under subdued light. 3 µl of Donor Mix ((Dilution buffer + AlphaScreen® Donor beads, PerkinElmer 6760002) were added per well and plates shaken for 1 minute. After 2 hours at RT plates were read on an Envision2 (PerkinElmer) using standard 384 AlphaScreen settings. The raw data were imported into and analyzed with the Boehringer Ingelheim proprietary software MegaLab (curve fitting based on the program PRISM, GraphPad Inc.).

Proliferation assays with A431 and PC-9$^{del19\ T790M\ C797S}$ cells

A431 cells were obtained from ATCC (CRL-1555 Lot# 1179038) and cultured in DMEM containing 10% FBS and supplemented with Sodium Pyruvate. Parental PC-9 cells were purchased from ECACC (90071810 Lot# 14A030) and cultured in RPMI (Gibco 61870) containing 10% FBS. Genome engineering was used to insert the mutations T790M and C797S into exon 20 of the endogenous EGFR locus resulting in the isolation of the PC-9$^{del19\ T790M\ C797S}$ variant. Successful introduction of the two mutations was verified using DNA sequencing, RNA sequencing and dose-response treatments with EGFR TKI.

5000 A431 cells and 2000 PC-9$^{del19\ T790M\ C797S}$ cells were plated per well in a 96-well plate. 24h after plating, cells were treated with compounds. All treatments were performed in technical and biological triplicates. Treated cells were incubated for 96h at 37°C with 5% CO_2. CellTiter-Glo® Luminescent Cell Viability Assay (Promega, #G7572) was performed and luminescence signal were detected by using the multilabel Plate Reader VICTOR X4. Quantifications of viable cells were calculated by normalization of compound treated

cells to DMSO treated cells. IC50 values were calculated using Megalab Software (Boehringer Ingelheim).

In-vivo studies in mice

Mice were group-housed (8-10 mice per cage) under pathogen-free and controlled environmental conditions (21 ± 1.5°C temperature, 55 ± 10% humidity) and handled according to the institutional, governmental and European Union guidelines (Austrian Animal Protection Laws, GV-SOLAS and FELASA guidelines). Animal studies were approved by the internal ethics committee and the local governmental committee. For the biomarker and xenograft studies, 6-8 week old, female BomTac:NMRI-*Foxn1*^{nu} mice; Taconic, Denmark) were engrafted subcutaneously with 5×10^6 PC-9$^{del19\ T790M\ C797S}$ cells. Animals were randomized according to tumor size 7 days after cell injection (N=8/group for compound and N=10 for vehicle treated mice). Animals were treated daily with 25 mg/kg osimertinib, 10 mg/kg BI-4020 or with the vehicle (Natrosol 0.5 %) only. Tumor size and body weight were measured three times weekly. Animals were examined daily

and sacrificed based on severity criteria including tumor size exceeding 1500 mm^3 or tumor necrosis. For the biomarker experiment animals were randomized 17 days after cell injection (N=4) and once treated one day later with 10 mg/kg BI -4020 or with the vehicle only. Tumor samples were harvested 6, 18 and 24h later and frozen in liquid nitrogen for analysis.

One-sided decreasing Mann–Whitney tests were used to compare tumor volumes. The p values were adjusted for multiple comparisons according to Bonferroni–Holm. For all analysis, p values under 0.05 represented a statistically significant effect.

In-vivo p-EGFR biomarker experiments

Proteins from PC-$9^{del19\ T790M\ C797S}$ tumor samples were extracted using ReadyPrep™ Mini Grinders (BioRad, #1632146). Tumor tissue was disrupted with a pestle in Tris Lysis Buffer (MSD, #R60TX-2) supplemented with Halt™ Protease and Phosphatase Inhibitor Cocktail (100X) (Thermo Scientific™, #78446). After 10min of incubation on ice, samples were centrifuged at 13 000rpm for 5min at 4°C. Supernatant were shock

frozen in LN2 and stored at -80°C overnight. Protein concentrations were determined using Bradford assay. For Wes Protein Simple analysis 0.5 µg of total protein was analysed using EGFR, p-EGFR and GAPDH antibodies (EGF Receptor (D38B1) XP® Rabbit mAb #4267; Phospho-EGF Receptor (Tyr1068) (D7A5) XP® Rabbit mAb #3777, Cell Signaling Technology) (Anti-GAPDH antibody - Loading Control (ab9485), abam). Protein levels were quantified using Wes Protein Simple Compass Software.

DMPK Assays

Aqueous solubility were determined from 1 mg/mL solid compound dispensed into aqueous McIlvaine buffer (pH 4.5 or 6.8), or dissolved in acetonitrile/water (1:1) as reference. Dissolved concentrations were determined with an Agilent 1200 HPLC/DAD-UV system.

Plasma protein binding (PPB) was determined by equilibrium dialysis. Plasma was spiked with EGFR TKI and dialyzed against Soerensen buffer (pH 7.4) for 3 hours at 37°C. PPB

was calculated by quantifying EGFR TKI concentrations in plasma and buffer by HPLC/MS-MS. *In-vivo* hepatic clearance (CL) was predicted by *in-vitro* incubations of 1 µM EGFR TKI with cryopreserved hepatocytes (Celsis IVT) and measured depletion over 240 minutes by quantitation of EGFR TKI by LC/MS/MS and using the well-stirred model. Data for hepatic CL were reported as %QH values. %QH values were determined by normalizing the hepatic CL by the respective blood follow through the liver (e.g. 90 ml/min/kg for mouse, 20.7 ml/min/kg for human). For **BI-4020** the predicted CL by human hepatocytes is 9.7 ml/min/kg. This corresponds to a clearance of (9.7 ml/min/kg / 20.7 ml/min/kg = 0.47) 47% QH.

PAMPA parameters were determined by using a chamber separated by a microfilter disc (coated with structured layers of immobilized artificial phospholipid membranes) into a donor and an acceptor area. The time dependent compound concentrations between the two champers is measured by LC/MS and compared to the concentration in the donor compartment prior to incubation. From this information, the permeability coefficient through the artificial membrane is calculated.[65]

For mouse pharmacokinetics (PK) analysis NMRI mice (n=3 per group) were dosed with BI-4042 orally (10 mg/kg) or intravenously (1 mg/kg). Five plasma samples were obtained per mouse at defined time points. After precipitation of the plasma protein with acetonitrile, the concentrations of BI-4020 were measured using LC-MS/MS against a calibration curve to calculate the concentration in plasma. The obtained concentration-time profiles are displayed in **Supplementary Figure 4**.

AUTHOR INFORMATION

Corresponding Author

* Harald.Engelhardt@boehringer-ingelheim.com

Present Addresses

† Merck Healthcare KGaA, Frankfurter Str. 250, 64293 Darmstadt Germany.

Author Contributions

The manuscript was written through contributions of all authors. All authors have given approval to the final version of the manuscript. ‡These authors contributed equally.

Funding Sources

This work was supported by the Austrian Research Promotion Agency (FFG) [grant number 872827].

ACKNOWLEDGMENT

We would like to thank Amy Gao, Gabriele Glendinning, Christoph Harrer, Susanne Mayer, Julia Mosler, Scott Pennino, Christian Salamon, Markus Spina, Elisabeth Traxler, June Wang and Anika Weiss for excellent project support.

ABBREVIATIONS

HATU, 1-[Bis(dimethylamino)methylene]-1H-1,2,3-triazolo[4,5-b]pyridinium 3-oxid hexafluorophosphate.

X-ray COORDINATES

Coordinates and structure factors have been deposited at the PDB/CCDC with PDB/CCDC codes 6S9B (compound **1**), 6S9C (compound **5**), 6S9D (compound **6**) and 1941612 (compound **9Br**). Author will release coordinates and experimental data upon article is published.

ASSOCIATED CONTENT

Supporting Information

Details for the QM-calculation for figure 4 are given. Description of the analytic and preparative HPLC methods as well as synthesis and analytic data (RT, MS, HRMS and ^{1}H NMR) of compounds **13a**, **13e**, **16b**, **16c**, **20a**, **20b**, **22b**, **22c**, **24**, **25a**, **25**, **26**, **34**, **35**, **35a**, **36**, **37**, **39**, **40**, **43** and **44** are given. Also X-ray data collection and refinement statistics for compound **1**, **5**, **6** and **9Br** are provided. HPLC-traces for compounds **1**, **2**, **3**, **3a**, **4**, **5**, **6**, **7**, **8**, **9**, **9Br** and **BI-4020** are shown. Molecular-formula strings are also provided. Furthermore the list of kinases of the kinase selectivity panels are given. Biochemical data for **6** – **BI-4020** and PK graphs of **BI-4020** are provided.

This material is available free of charge via the Internet at http://pubs.acs.org.

REFERENCES

1. Roskoski, R. J. There are 49 FDA-Approved Small Molecule Protein Kinase Inhibitors as of 12 April 2019. http://www.brimr.org/PKI/PKIs.htm (accessed Mai 3, 2019).
2. Smyth, L. A.; Collins, I., Measuring and Interpreting the Selectivity of Protein Kinase Inhibitors. *Journal of chemical biology* **2009,** *2* (3), 131-151.
3. Anastassiadis, T.; Deacon, S. W.; Devarajan, K.; Ma, H.; Peterson, J. R., Comprehensive Assay of Kinase Catalytic Activity Reveals Features of Kinase Inhibitor Selectivity. *Nature biotechnology* **2011,** *29* (11), 1039.
4. Tang, Z. H.; Lu, J. J., Osimertinib Resistance in Non-Small Cell Lung Cancer: Mechanisms and Therapeutic Strategies. *Cancer Letters* **2018,** *420*, 242-246.
5. Ricordel, C.; Friboulet, L.; Facchinetti, F.; Soria, J. C., Molecular Mechanisms of Acquired Resistance to Third-Generation EGFR-TKIs in EGFR T790M-Mutant Lung Cancer. *Annals of Oncology* **2018,** *29*, i28-i37.
6. Lategahn, J.; Keul, M.; Rauh, D., Lessons to be Learned: The Molecular Basis of Kinase-Targeted Therapies and Drug Resistance in Non-Small Cell Lung Cancer. *Angewandte Chemie - International Edition* **2018,** *57* (9), 2307-2313.
7. Zhu, S. J.; Zhao, P.; Yang, J.; Ma, R.; Yan, X. E.; Yang, S. Y.; Yang, J. W.; Yun, C. H., Structural Insights into Drug Development Strategy Targeting EGFR T790M/C797S. *Oncotarget* **2018,** *9* (17), 13652-13665.
8. Elkins, J. M.; Fedele, V.; Szklarz, M.; Abdul Azeez, K. R.; Salah, E.; Mikolajczyk, J.; Romanov, S.; Sepetov, N.; Huang, X.-P.; Roth, B. L.; Al Haj Zen, A.; Fourches, D.; Muratov, E.; Tropsha, A.; Morris, J.; Teicher, B. A.; Kunkel, M.; Polley, E.; Lackey, K. E.; Atkinson, F. L.; Overington, J. P.; Bamborough, P.; Muller, S.; Price, D. J.; Willson, T. M.; Drewry, D. H.; Knapp, S.; Zuercher, W. J., Comprehensive Characterization of the Published Kinase Inhibitor Set. *Nat. Biotechnol.* **2016,** *34* (1), 95-103.
9. Drewry, D. H.; Wells, C. I.; Andrews, D. M.; Angell, R.; Al-Ali, H.; Axtman, A. D.; Capuzzi, S. J.; Elkins, J. M.; Ettmayer, P.; Frederiksen, M.; Gileadi, O.; Gray, N.; Hooper, A.; Knapp, S.; Laufer, S.; Luecking, U.; Mueller, S.; Muratov, E.; Denny, R. A.; Saikatendu, K. S.; Treiber, D. K.; Zuercher, W. J.; Willson, T. M., Progress Towards a Public Chemogenomic Set for Protein Kinases and a Call for Contributions. *bioRxiv, Pharmacol. Toxicol.* **2017**, 1-21.
10. Driggers, E. M.; Hale, S. P.; Lee, J.; Terrett, N. K., The Exploration of Macrocycles for Drug Discovery - An Underexploited Structural Class. *Nature Reviews Drug Discovery* **2008,** *7* (7), 608-624.
11. Johnson, T. W.; Richardson, P. F.; Bailey, S.; Brooun, A.; Burke, B. J.; Collins, M. R.; Cui, J. J.; Deal, J. G.; Deng, Y.-L.; Dinh, D.; Engstrom, L. D.; He, M.; Hoffman, J.; Hoffman, R. L.; Huang, Q.; Kania, R. S.; Kath, J. C.; Lam, H.; Lam, J. L.; Le, P. T.; Lingardo, L.; Liu, W.; McTigue, M.; Palmer, C. L.; Sach, N. W.; Smeal, T.; Smith, G. L.; Stewart, A. E.; Timofeevski, S.; Zhu, H.; Zhu, J.; Zou, H. Y.; Edwards, M. P., Discovery of (10R)-7-Amino-12-fluoro-2,10,16-trimethyl-15-oxo-10,15,16,17-tetrahydro-2H-8,4-(metheno)pyrazolo[4,3-h][2,5,11]-benzoxadiazacyclotetradecine-3-carbonitrile (PF-06463922), a Macrocyclic Inhibitor of Anaplastic Lymphoma Kinase (ALK) and c-ros Oncogene 1 (ROS1) with Preclinical Brain

Exposure and Broad-Spectrum Potency against ALK-Resistant Mutations. *J. Med. Chem.* **2014,** *57* (11), 4720-4744.
12. Midha, A.; Dearden, S.; McCormack, R., EGFR Mutation Incidence in Non-Small-Cell Lung Cancer of Adenocarcinoma Histology: a Systematic Review and Global Map by Ethnicity (mutMapII). *Am J Cancer Res* **2015,** *5* (9), 2892-2911.
13. Konduri, K.; Gallant, J.-N.; Chae, Y. K.; Giles, F. J.; Gitlitz, B. J.; Gowen, K.; Ichihara, E.; Owonikoko, T. K.; Peddareddigari, V.; Ramalingam, S. S.; Reddy, S. K.; Eaby-Sandy, B.; Vavala, T.; Whiteley, A.; Chen, H.; Yan, Y.; Sheehan, J. H.; Meiler, J.; Morosini, D.; Ross, J. S.; Stephens, P. J.; Miller, V. A.; Ali, S. M.; Lovly, C. M., EGFR Fusions as Novel Therapeutic Targets in Lung Cancer. *Cancer Discovery* **2016,** *6* (6), 601-611.
14. Mitsudomi, T.; Morita, S.; Yatabe, Y.; Negoro, S.; Okamoto, I.; Tsurutani, J.; Seto, T.; Satouchi, M.; Tada, H.; Hirashima, T.; Asami, K.; Katakami, N.; Takada, M.; Yoshioka, H.; Shibata, K.; Kudoh, S.; Shimizu, E.; Saito, H.; Toyooka, S.; Nakagawa, K.; Fukuoka, M., Gefitinib Versus Cisplatin Plus Docetaxel in Patients With Non-Small-Cell Lung Cancer Harboring Mutations of the Epidermal Growth Factor Receptor (WJTOG3405): an Open Label, Randomised Phase 3 trial. *Lancet Oncol.* **2010,** *11* (2), 121-128.
15. Park, K.; Tan, E.-H.; O'Byrne, K.; Zhang, L.; Boyer, M.; Mok, T.; Hirsh, V.; Yang, J. C.-H.; Lee, K. H.; Lu, S.; Shi, Y.; Kim, S.-W.; Laskin, J.; Kim, D.-W.; Arvis, C. D.; Kolbeck, K.; Laurie, S. A.; Tsai, C.-M.; Shahidi, M.; Kim, M.; Massey, D.; Zazulina, V.; Paz-Ares, L., Afatinib Versus Gefitinib as First-Line Treatment of Patients with EGFR Mutation-Positive Non-Small-Cell Lung Cancer (LUX-Lung 7): a Phase 2B, Open-Label, Randomised Controlled Trial. *Lancet Oncol.* **2016,** *17* (5), 577-589.
16. Soria, J. C.; Ohe, Y.; Vansteenkiste, J.; Reungwetwattana, T.; Chewaskulyong, B.; Lee, K. H.; Dechaphunkul, A.; Imamura, F.; Nogami, N.; Kurata, T.; Okamoto, I.; Zhou, C.; Cho, B. C.; Cheng, Y.; Cho, E. K.; Voon, P. J.; Planchard, D.; Su, W. C.; Gray, J. E.; Lee, S. M.; Hodge, R.; Marotti, M.; Rukazenkov, Y.; Ramalingam, S. S., Osimertinib in Untreated EGFR-Mutated Advanced Non-Small-Cell Lung Cancer. *N. Engl. J. Med.* **2018,** *378* (2), 113-125.
17. Zhou, C.; Wu, Y.-L.; Chen, G.; Feng, J.; Liu, X.-Q.; Wang, C.; Zhang, S.; Wang, J.; Zhou, S.; Ren, S.; Lu, S.; Zhang, L.; Hu, C.; Hu, C.; Luo, Y.; Chen, L.; Ye, M.; Huang, J.; Zhi, X.; Zhang, Y.; Xiu, Q.; Ma, J.; Zhang, L.; You, C., Erlotinib Versus Chemotherapy as First-Line Treatment for Patients with Advanced EGFR Mutation-Positive Non-Small-Cell Lung Cancer (OPTIMAL, CTONG-0802): a Multicentre, Open-Label, Randomised, Phase 3 Study. *Lancet Oncol.* **2011,** *12* (8), 735-742.
18. Wu, Y.-L.; Cheng, Y.; Zhou, X.; Lee, K. H.; Nakagawa, K.; Niho, S.; Tsuji, F.; Linke, R.; Rosell, R.; Corral, J.; Migliorino, M. R.; Pluzanski, A.; Sbar, E. I.; Wang, T.; White, J. L.; Nadanaciva, S.; Sandin, R.; Mok, T. S., Dacomitinib Versus Gefitinib as First-Line Treatment for Patients with EGFR-Mutation-Positive Non-Small-Cell Lung Cancer (ARCHER 1050): a Randomised, Open-Label, Phase 3 Trial. *Lancet Oncol.* **2017,** *18* (11), 1454-1466.
19. Blakely, C. M.; Bivona, T. G., Resiliency of Lung Cancers to EGFR Inhibitor Treatment Unveiled, Offering Opportunities to Divide and Conquer EGFR Inhibitor Resistance. *Cancer Discovery* **2012,** *2* (10), 872-875.
20. Kobayashi, S.; Boggon, T. J.; Dayaram, T.; Jaenne, P. A.; Kocher, O.; Meyerson, M.; Johnson, B. E.; Eck, M. J.; Tenen, D. G.; Halmos, B., EGFR Mutation and Resistance of Non-Small-Cell Lung Cancer to Gefitinib. *N. Engl. J. Med.* **2005,** *352* (8), 786-792.
21. Wang, S.; Cang, S.; Liu, D., Third-Generation Inhibitors Targeting EGFR T790M Mutation in Advanced Non-Small Cell Lung Cancer. *J. Hematol. Oncol.* **2016,** *9*, 34/1-34/7.

22. Cross, D. A. E.; Ashton, S. E.; Ghiorghiu, S.; Eberlein, C.; Nebhan, C. A.; Spitzler, P. J.; Orme, J. P.; Finlay, M. R. V.; Ward, R. A.; Mellor, M. J.; Hughes, G.; Rahi, A.; Jacobs, V. N.; Brewer, M. R.; Ichihara, E.; Sun, J.; Jin, H.; Ballard, P.; Al-Kadhimi, K.; Rowlinson, R.; Klinowska, T.; Richmond, G. H. P.; Cantarini, M.; Kim, D.-W.; Ranson, M. R.; Pao, W., AZD9291, an Irreversible EGFR TKI, Overcomes T790M-Mediated Resistance to EGFR Inhibitors in Lung Cancer. *Cancer Discovery* **2014,** *4* (9), 1046-1061.
23. Janne, P. A.; Yang, J. C.-H.; Kim, D.-W.; Planchard, D.; Ohe, Y.; Ramalingam, S. S.; Ahn, M.-J.; Kim, S.-W.; Su, W.-C.; Horn, L.; Haggstrom, D.; Felip, E.; Kim, J.-H.; Frewer, P.; Cantarini, M.; Brown, K. H.; Dickinson, P. A.; Ghiorghiu, S.; Ranson, M., AZD9291 in EGFR Inhibitor-Resistant Non-Small-Cell Lung Cancer. *N Engl J Med* **2015,** *372* (18), 1689-1699.
24. Mok, T. S.; Wu, Y. L.; Ahn, M. J.; Garassino, M. C.; Kim, H. R.; Ramalingam, S. S.; Shepherd, F. A.; He, Y.; Akamatsu, H.; Theelen, W. S. M. E.; Lee, C. K.; Sebastian, M.; Templeton, A.; Mann, H.; Marotti, M.; Ghiorghiu, S.; Papadimitrakopoulou, V. A., Osimertinib or Platinum-Pemetrexed in EGFR T790M-Positive Lung Cancer. *N. Engl. J. Med.* **2017,** *376* (7), 629-640.
25. Ortiz-Cuaran, S.; Scheffler, M.; Plenker, D.; Dahmen, l.; Scheel, A. H.; Fernandez-Cuesta, L.; Meder, L.; Lovly, C. M.; Persigehl, T.; Merkelbach-Bruse, S.; Bos, M.; Michels, S.; Fischer, R.; Albus, K.; Koenig, K.; Schildhaus, H.-U.; Fassunke, J.; Ihle, M. A.; Pasternack, H.; Heydt, C.; Becker, C.; Altmueller, J.; Ji, H.; Mueller, C.; Florin, A.; Heuckmann, J. M.; Nuernberg, P.; Ansen, S.; Heukamp, L. C.; Berg, J.; Pao, W.; Peifer, M.; Buettner, R.; Wolf, J.; Thomas, R. K.; Sos, M. L., Heterogeneous Mechanisms of Primary and Acquired Resistance to Third-Generation EGFR Inhibitors. *Clin. Cancer Res.* **2016,** *22* (19), 4837-4847.
26. Song, H.-N.; Jung, K. S.; Yoo, K. H.; Cho, J.; Lee, J. Y.; Lim, S. H.; Kim, H. S.; Sun, J.-M.; Lee, S.-H.; Ahn, J. S.; Park, K.; Choi, Y.-L.; Park, W.; Ahn, M.-J., Acquired C797S Mutation upon Treatment with a T790M-Specific Third-Generation EGFR Inhibitor (HM61713) in Non-Small Cell Lung Cancer. *J Thorac Oncol* **2016,** *11* (4), e45-e47.
27. Thress, K. S.; Paweletz, C. P.; Felip, E.; Cho, B. C.; Stetson, D.; Dougherty, B.; Lai, Z.; Markovets, A.; Vivancos, A.; Kuang, Y.; Ercan, D.; Matthews, S. E.; Cantarini, M.; Barrett, J. C.; Janne, P. A.; Oxnard, G. R., Acquired EGFR C797S Mutation Mediates Resistance to AZD9291 in Non-Small Cell Lung Cancer Harboring EGFR T790M. *Nat. Med. (N. Y., NY, U. S.)* **2015,** *21* (6), 560-562.
28. Yang, Z.; Yang, N.; Ou, Q.; Xiang, Y.; Jiang, T.; Wu, X.; Bao, H.; Tong, X.; Wang, X.; Shao, Y. W.; Liu, Y.; Wang, Y.; Zhou, C., Investigating Novel Resistance Mechanisms to Third-Generation EGFR Tyrosine Kinase Inhibitor Osimertinib in Non-Small Cell Lung Cancer Patients. *Clin. Cancer Res.* **2018,** *24* (13), 3097-3107.
29. Yu, H. A.; Drilon, A. E.; Riely, G. J.; Tian, S. K.; Borsu, L.; Arcila, M. E.; Ladanyi, M., Acquired Resistance of EGFR-Mutant Lung Cancer to a T790M-Specific EGFR Inhibitor: Emergence of a Third Mutation (C797S) in the EGFR Tyrosine Kinase Domain. *JAMA Oncol* **2015,** *1* (7), 982-984.
30. Ramalingam, S. S.; Yang, J. C. H.; Lee, C. K.; Kurata, T.; Kim, D.-W.; John, T.; Nogami, N.; Ohe, Y.; Mann, H.; Rukazenkov, Y.; Ghiorghiu, S.; Stetson, D.; Markovets, A.; Carl Barrett, J.; Thress, K. S.; Jaenne, P. A., Osimertinib as First-Line Treatment of EGFR Mutation-Positive Advanced Non-Small-Cell Lung Cancer. *J. Clin. Oncol.* **2018,** *36* (9), 841-849.

31. Hei, Y. Y.; Shen, Y.; Wang, J.; Zhang, H.; Zhao, H. Y.; Xin, M.; Cao, Y. X.; Li, Y.; Zhang, S. Q., Synthesis and Evaluation of 2,9-Disubstituted 8-Phenylthio/Phenylsulfinyl-9H-Purine as New EGFR Inhibitors. *Bioorg. Med. Chem.* **2018,** *26* (8), 2173-2185.
32. Chen, L.; Zhang, Y.; Liu, J.; Wang, W.; Li, X.; Zhao, L.; Wang, W.; Li, B., Novel 4-Arylaminoquinazoline Derivatives with (E)-Propen-1-yl moiety as Potent EGFR Inhibitors with Enhanced Antiproliferative Activities Against Tumor Cells. *Eur. J. Med. Chem.* **2017,** *138* (Supplement C), 689-697.
33. Günther, M.; Lategahn, J.; Juchum, M.; Döring, E.; Keul, M.; Engel, J.; Tumbrink, H. L.; Rauh, D.; Laufer, S., Trisubstituted Pyridinylimidazoles as Potent Inhibitors of the Clinically Resistant L858R/T790M/C797S EGFR Mutant: Targeting of Both Hydrophobic Regions and the Phosphate Binding Site. *J. Med. Chem.* **2017,** *60* (13), 5613-5637.
34. Fukuda, T.; Umeki, T.; Tokushima, K.; Xiang, G.; Yoshida, Y.; Ishibashi, F.; Oku, Y.; Nishiya, N.; Uehara, Y.; Iwao, M., Design, Synthesis, and Evaluation of A-Ring-Modified Lamellarin N Analogues as Noncovalent Inhibitors of the EGFR T790M/L858R Mutant. *Biorg. Med. Chem.* **2017**, 25(24), 6563-5680.
35. Zhang, H.; Wang, J.; Shen, Y.; Wang, H. Y.; Duan, W. M.; Zhao, H. Y.; Hei, Y. Y.; Xin, M.; Cao, Y. X.; Zhang, S. Q., Discovery of 2,4,6-Trisubstitued Pyrido[3,4-d]pyrimidine Derivatives as new EGFR-TKIs. *Eur. J. Med. Chem.* **2018,** *148*, 221-237.
36. Juchum, M.; Günther, M.; Döring, E.; Sievers-Engler, A.; Lämmerhofer, M.; Laufer, S., Trisubstituted Imidazoles with a Rigidized Hinge Binding Motif Act As Single Digit nM Inhibitors of Clinically Relevant EGFR L858R/T790M and L858R/T790M/C797S Mutants: An Example of Target Hopping. *J. Med. Chem.* **2017,** *60* (11), 4636-4656.
37. Lu, X.; Zhang, T.; Zhu, S.-J.; Xun, Q.; Tong, L.; Hu, X.; Li, Y.; Chan, S.; Su, Y.; Sun, Y.; Chen, Y.; Ding, J.; Yun, C.-H.; Xie, H.; Ding, K., Discovery of JND3229 as a New EGFRC797S Mutant Inhibitor with In Vivo Monodrug Efficacy. *ACS Med. Chem. Lett.* **2018,** *9* (11), 1123-1127.
38. Hanan, E. J.; Baumgardner, M.; Bryan, M. C.; Chen, Y.; Eigenbrot, C.; Fan, P.; Gu, X. H.; La, H.; Malek, S.; Purkey, H. E.; Schaefer, G.; Schmidt, S.; Sideris, S.; Yen, I.; Yu, C.; Heffron, T. P., 4-Aminoindazolyl-dihydrofuro[3,4-d]pyrimidines as Non-cCvalent Inhibitors of Mutant Epidermal Growth Factor Receptor Tyrosine Kinase. *Bioorg. Med. Chem. Lett.* **2016,** *26* (2), 534-539.
39. Heald, R.; Bowman, K. K.; Bryan, M. C.; Burdick, D.; Chan, B.; Chan, E.; Chen, Y.; Clausen, S.; Dominguez-Fernandez, B.; Eigenbrot, C.; Elliott, R.; Hanan, E. J.; Jackson, P.; Knight, J.; La, H.; Lainchbury, M.; Malek, S.; Mann, S.; Merchant, M.; Mortara, K.; Purkey, H.; Schaefer, G.; Schmidt, S.; Seward, E.; Sideris, S.; Shao, L.; Wang, S.; Yeap, K.; Yen, I.; Yu, C.; Heffron, T. P., Noncovalent Mutant Selective Epidermal Growth Factor Receptor Inhibitors: A Lead Optimization Case Study. *J. Med. Chem.* **2015,** *58* (22), 8877-8895.
40. Hanan, E. J.; Eigenbrot, C.; Bryan, M. C.; Burdick, D. J.; Chan, B. K.; Chen, Y.; Dotson, J.; Heald, R. A.; Jackson, P. S.; La, H.; Lainchbury, M. D.; Malek, S.; Purkey, H. E.; Schaefer, G.; Schmidt, S.; Seward, E. M.; Sideris, S.; Tam, C.; Wang, S.; Yeap, S. K.; Yen, I.; Yin, J.; Yu, C.; Zilberleyb, I.; Heffron, T. P., Discovery of Selective and Noncovalent Diaminopyrimidine-Based Inhibitors of Epidermal Growth Factor Receptor Containing the T790M Resistance Mutation. *J. Med. Chem.* **2014,** *57* (23), 10176-10191.
41. Bryan, M. C.; Burdick, D. J.; Chan, B. K.; Chen, Y.; Clausen, S.; Dotson, J.; Eigenbrot, C.; Elliott, R.; Hanan, E. J.; Heald, R.; Jackson, P.; La, H.; Lainchbury, M.; Malek, S.; Mann, S. E.; Purkey, H. E.; Schaefer, G.; Schmidt, S.; Seward, E.; Sideris, S.; Wang, S.; Yen, I.; Yu, C.;

Heffron, T. P., Pyridones as Highly Selective, Noncovalent Inhibitors of T790M Double Mutants of EGFR. *ACS Med. Chem. Lett.* **2016,** *7* (1), 100-104.
42. Park, H.; Jung, H.-Y.; Mah, S.; Hong, S., Discovery of EGF Receptor Inhibitors That Are Selective for the d746-750/T790M/C797S Mutant through Structure-Based de Novo Design. *Angew. Chem. Int. Ed.* **2017,** *56* (26), 7634-7638.
43. Chan, B. K.; Hanan, E. J.; Bowman, K. K.; Bryan, M. C.; Burdick, D.; Chan, E.; Chen, Y.; Clausen, S.; Dela Vega, T.; Dotson, J.; Eigenbrot, C.; Elliott, R. L.; Heald, R. A.; Jackson, P. S.; Knight, J. D.; La, H.; Lainchbury, M. D.; Malek, S.; Purkey, H. E.; Schaefer, G.; Schmidt, S.; Seward, E. M.; Sideris, S.; Shao, L.; Wang, S.; Yeap, S. K.; Yen, I.; Yu, C.; Heffron, T. P., Discovery of a Noncovalent, Mutant-Selective Epidermal Growth Factor Receptor Inhibitor. *J. Med. Chem.* **2016,** *59* (19), 9080-9093.
44. Patel, H. M.; Pawara, R.; Ansari, A.; Noolvi, M.; Surana, S., Design and Synthesis of Quinazolinones as EGFR Inhibitors to Overcome EGFR Resistance Obstacle. *Biorg. Med. Chem.* **2017,** *25* (10), 2713-2723.
45. Wang, S.; Song, Y.; Liu, D., EAI045: The Fourth-Generation EGFR Inhibitor Overcoming T790M and C797S resistance. *Cancer Letters* **2017,** *385*, 51-54.
46. Spellmon, N.; Li, C.; Yang, Z., Allosterically Targeting EGFR Drug-Resistance Gatekeeper Mutations. *Journal of Thoracic Disease* **2017,** *9* (7), 1756-1758.
47. Kannan, S.; Venkatachalam, G.; Lim, H. H.; Surana, U.; Verma, C., Conformational Landscape of the Epidermal Growth Factor Receptor Kinase Reveals a Mutant Specific Allosteric Pocket. *Chemical Science* **2018,** *9* (23), 5212-5222.
48. Caporuscio, F.; Tinivella, A.; Restelli, V.; Semrau, M. S.; Pinzi, L.; Storici, P.; Broggini, M.; Rastelli, G., Identification of Small-Molecule EGFR Allosteric Inhibitors by High-Throughput Docking. *Future Medicinal Chemistry* **2018,** *10* (13), 1545-1553.
49. Zhao, P.; Yao, M. Y.; Zhu, S. J.; Chen, J. Y.; Yun, C. H., Crystal Structure of EGFR T790M/C797S/V948R in Complex with EAI045. *Biochem. Biophys. Res. Commun.* **2018,** *502* (3), 332-337.
50. To determine the kinase selectivity for a given compound the "SelectScreen Kinase Profiling Services" from ThermoFisher was used. The activity of a compound was determined in biochemical assays using single concentration measurements. The results were provided as percent inhibition values. A compound displaying a percent inhibition value of greater 70% was defined as hit. Three different kinase panels were used (30 kinases, 238 kinases and 393 kinases) and the list of kinases for this repective panels are provided in the supporting information (**Supplementary Table 5-7**). The $EGFR^{L858R\ T790M\ C797S}$ kinase assay was used as positive control.
51. Traxler, P.; Furet, P., Strategies Toward the Design of Novel and Selective Protein Tyrosine Kinase Inhibitors. *Pharmacol. Ther.* **1999,** *82* (2-3), 195-206.
52. Chai, J.-D.; Head-Gordon, M., Long-range Corrected Hybrid Density Functionals With Damped Atom-Atom Dispersion Corrections. *Phys. Chem. Chem. Phys.* **2008,** *10* (44), 6615-6620.
53. Alihodžić, S.; Bukvić, M.; Elenkov, I. J.; Hutinec, A.; Koštrun, S.; Pešić, D.; Saxty, G.; Tomašković, L.; Žiher, D., Current Trends in Macrocyclic Drug Discovery and Beyond-Ro5. In *Prog. Med. Chem.*, 2018; Vol. 57, pp 113-233.
54. Whitty, A.; Viarengo, L. A.; Zhong, M., Progress Towards the Broad Use of Non-Peptide Synthetic Macrocycles in Drug Discovery. *Org. Biomol. Chem.* **2017,** *15* (37), 7729-7735.

55. Ermert, P., Design, Properties and Recent Application of Macrocycles in Medicinal Chemistry. *Chimia* **2017,** *71* (10), 678-702.
56. Labute, P., LowModeMD - Implicit Low-Mode Velocity Filtering Applied to Conformational Search of Macrocycles and Protein Loops. *J. Chem. Inf. Model.* **2010,** *50* (5), 792-800.
57. Kamenik, A. S.; Lessel, U.; Fuchs, J. E.; Fox, T.; Liedl, K. R., Peptidic Macrocycles - Conformational Sampling and Thermodynamic Characterization. *J. Chem. Inf. Model.* **2018,** *58* (5), 982-992.
58. Klebl, B.; Mueller, G.; Hamacher, M.; Editors, *Protein Kinases as Drug Targets. [In: Methods Princ. Med. Chem., 2011; 49]*. Wiley-VCH Verlag GmbH & Co. KGaA, Weinheim: 2011; p 373 pp.
59. Baell, J. B.; Nissink, J. W. M., Seven Year Itch: Pan-Assay Interference Compounds (PAINS) in 2017-Utility and Limitations. *ACS Chem. Biol*. **2018**, 13 (1), 36-44.
60. Baell, J. B.; Holloway, G. A., New Substructure Filters for Removal of Pan Assay Interference Compounds (PAINS) from Screening Libraries and for Their Exclusion in Bioassays. *J. Med. Chem.* **2010**, 53 (7), 2719-2740.
61. Hanan, E. J.; Eigenbrot, C.; Bryan, M. C.; Burdick, D. J.; Chan, B. K.; Chen, Y.; Dotson, J.; Heald, R. A.; Jackson, P. S.; La, H.; Lainchbury, M. D.; Malek, S.; Purkey, H. E.; Schaefer, G.; Schmidt, S.; Seward, E. M.; Sideris, S.; Tam, C.; Wang, S.; Yeap, S. K.; Yen, I.; Yin, J.; Yu, C.; Zilberleyb, I.; Heffron, T. P., Discovery of Selective and Noncovalent Diaminopyrimidine-Based Inhibitors of Epidermal Growth Factor Receptor Containing the T790M Resistance Mutation. *J. Med. Chem.* **2014**, 57 (23), 10176-10191.
62. Kabsch, W., XDS. *Acta Crystallogr D Biol Crystallogr* **2010**, 66 (Pt 2), 125-132.
63. Winn, M. D.; Ballard, C. C.; Cowtan, K. D.; Dodson, E. J.; Emsley, P.; Evans, P. R.; Keegan, R. M.; Krissinel, E. B.; Leslie, A. G. W.; McCoy, A.; McNicholas, S. J.; Murshudov, G. N.; Pannu, N. S.; Potterton, E. A.; Powell, H. R.; Read, R. J.; Vagin, A.; Wilson, K. S., Overview of the CCP4 Suite and Current Developments. *Acta Crystallogr., Sect. D: Biol. Crystallogr.* **2011**, 67 (4), 235-242.
64. Vagin, A. A.; Steiner, R. A.; Lebedev, A. A.; Potterton, L.; McNicholas, S.; Long, F.; Murshudov, G. N., REFMAC5 Dictionary: Organization of Prior Chemical Knowledge and Guidelines for its Use. *Acta Crystallogr., Sect. D: Biol. Crystallogr.* **2004**, D60 (12, Pt. 1), 2184-2195.
65. Luippold, A. H.; Arnhold, T.; Joerg, W.; Krueger, B.; Suessmuth, R. D., Application of a Rapid and Integrated Analysis System (RIAS) as a High-Throughput Processing Tool For In Vitro ADME Samples by Liquid Chromatography/tandem Mass Spectrometry. *J. Biomol. Screening* **2011,** *16* (3), 370-377.

For Table of Contents Only

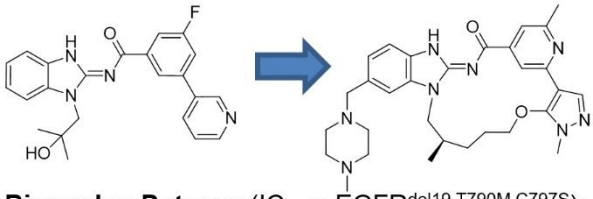

Biomarker Potency (IC_{50} p-$EGFR^{del19\ T790M\ C797S}$):

790 nM | 0.6 nM

EGFR wt-sparing ratio:

>400 | >400